The Effects of Obesity on Protein Corona Formation

Ville Papić

DIVISION OF FOOD AND PHARMA | DEPARTMENT OF PROCESS AND LIFE SCIENCE ENGINEERING FACULTY OF ENGINEERING LTH | LUND UNIVERSITY
2026

MASTER THESIS

The Effects of Obesity on Protein Corona Formation

Ville Papić

LUND
UNIVERSITY

The Effects of Obesity on Protein Corona Formation

Published by
Department of Process and Life Science Engineering
Faculty of Engineering LTH, Lund University
P.O. Box 118, SE-221 00 Lund, Sweden

Subject: KLGM16 Degree Project in Pharmaceutical Formulation

Division: Food and Pharma
Supervisor: Lars Nilsson
Examiner: Marie Wahlgren

The Effects of Obesity on Protein Corona Formation

by

Ville Papić

Process and Life Science Engineering

June 2026

Supervisor: Lars Nilsson
Examiner: Marie Wahlgren

Kan siffran på vågen påverka oss mer än vi trott?

Övervikt är något som vi alla kan råka drabbas av. Flera olika anledningar och orsaker kan få oss att lägga på något extra kilo här och där. De här små ökningarna har inga större effekter på oss, men det är när dessa små ökningar får låtas bli en stor ökning som det kan påverka oss negativt. Och under de senaste årtioden så har allt fler och fler personer blivit så pass överviktiga att de klassas som obesa, vilket är en trend som ser ut att fortsätta. Men förutom de effekter som vi redan känner till att övervikt för med sig, finns det några som påverkar oss utan att vi ens vet om att de finns?

Det är nog inget kontroversiellt påstående att övervikt och framför allt obesitas är dåligt för vår hälsa, särskillt när det sistnämnda har klassats som en sjukdom av bland annat världshälsoorganisationen (WHO). Det kan föra med sig en mängd av olika negativa effekter och öka risken för flera olika andra sjukdomar och åkommor. För dessa effekter kan en drabbad person behöva ta olika mediciner, till exempel mot högt blodtryck, högt blodsocker, och smärta. Men kan obesitas också påverka medicinerna som försöker lindra dess effekter?

Många läkemedel använder sig av väldigt väldigt små partiklar för att frakta runt det i kroppen. Dessa partiklarna, som kallas nanopartiklar, används bland annat för att skydda känsliga molekyler, se till så att läkemedlet kommer till rätt ställe, och att det inte släpps ut innan det kommer dit det ska. Men det är inte bara så lätt att de här partiklarna kommer in i kroppen och gör exakt vad de ska, utan det finns saker som kan sätta stop för det. För när partiklarna färdas i blodet på väg mot sitt mål så kan proteiner i blodplasman fästa sig på dem och ändra vart de tar vägen. Man kan tänka på det som hur att ändra formen på en nyckel påverkar vilken dörr den kan öppna. Detta experimentet avsåg att ta reda på hur övervikt och obesitas kan påverka vilka proteiner som fäster på dessa små partiklar, då detta kan hjälpa oss att förutsäga hur läkemedel kommer att bete sig i kroppen hos de påverkade.

Det som upptäcktes var att obesitas ser ut att göra så att vissa proteiner fäster mer till partiklarna än vanligt. Proteinerna som var extra undersökta var ”apolipoproteiner” som vanligtvis binder till fettpartiklar och bestämmer vart de tar vägen. Så om fler av dessa proteiner fäster till partiklarna med läkemedel innuti så hamnar de troligtvis någonstans de inte var tänkta att hamna. En av dessa proteiner kan ta partiklarna till levern där de kan bli renade ur kroppen tidigare än tänkt. Av elva olika apolipoproteiner som undersöktes så fäste alla förutom två mer till partiklar i blodet från individer (råttor) med obesitas. Men vissa av dessa resultat borde nog tas med en nypa salt tills fler experiment har gjorts.

Abstract

Obesity is a disease that has experienced a significant world wide increase over the past decades, sometimes even being referred to as an epidemic. And while there are many serious and well known effects caused by obesity, there could be even more that we don't yet know about.

This experiment intends to study the change between protein corona formation around lipid nanoparticles incubated in plasma form a control group and obese group. The plasma samples came from rats and were collected and given to us by Novo Nordisk. Lipid nanoparticles were incubated in pooled plasma from several individuals for each group, allowing a protein corona to form. The samples were then separated, analysed, and fractioned using an AF4 setup with a multiangle light scattering detector, differential refractive index detector, and UV detector. The relevant fractions from each injection were collected and prepared for mass spectrometry. Novo Nordisk then collected the samples and analysed them using liquid chromatography coupled with tandem mass spectrometry.

The protein analysis mainly looked into the change in protein corona presence of apolipoproteins and certain immunoglobulin related proteins. Most apolipoproteins displayed an increased presence in the protein corona of particles incubated in plasma from the obese group, with the highest increase being in apolipoprotein C-IV with 85,34%. Apolipoprotein C-I did show a higher increase with 304,92%, but due to reproducibility problems combined with being such an extreme number, it was disregarded. Apolipoprotein E which is known to make lipid nanoparticle drugs accumulate in the liver also showed an increase of 6,95%. There was also a large decrease shown for the polymeric immunoglobulin receptor, with a protein corona presence 41,88% lower for the obese group as compared to the control group.

While there were some interesting and promising results, the data did overall suffer from reproducibility issues most likely due to a limited sample size, as there were only two replicates for each group. Future work should thus firstly focus on increasing the amount of data for each group in order to produce more conclusive results before focusing on other aspects.

Sammanfattning

Obesitas är en sjukdom som har fått en signifikand ökning världen över under de senaste årtionden, i sådan mån att det ibland kallas för en epidemi. Och medans det finns många seriösa och välkända effekter orsakade av obesitas så kan det finnas ännu fler vi ännu inte känner till.

Detta experimentet har som mål att studera skillnaden mellan proteinkoronabildningen runt nanolipidpartiklar inkuberade i plasma från en kontrollgrupp och en grupp med obesitas. Plasmaproverna kom från råttor och samlades och gavs till oss av Novo Nordisk. Nanolipidpartiklar inkuberades in poolad plasma från flertalet individer för varje grupp så att en proteinkorona bildades runt dem. Proverna blev sedan separerade, analyserade och fraktionerade med hjälp av en AF4 setup som inkluderade en multiangle light scattering detektor, differential refractive index detektor, och UV-detektor. De relevanta fraktionerna från varje injektion förberredes för masspektrometri. Novo Nordisk samlade sedan in proven och analyserade dem med hjälp av vätskekromatografi koplad till tandem-masspektrometri.

Proteinanalysen kollade främst på förändringen i mängden av apolipoproteiner och antikroppsrelaterade proteiner i proteinkoronan mellan de två grupperna. De flesta apolipoproteiner visade på en ökning i proteinkoronan för partiklarna inkuberade i plasman från gruppen med obesitas jämfört med kontrollgruppen. Den högsta ökningen var i apolipoprotein C-IV med 85,34%. Apolipoprotein C-I visade på en ökning med 304,92%, med på grund av en bristande reproducerbarhet kombinerat med att det är en ganska extrem siffra så ansågs detta resultatet ej som trovärdigt. Apolipoprotein E känns till kunna leda till en ackumulering av nanolipidpartiklar i levern visade också en ökning på 6,95%. Nivån av den polymeriska antikroppsreceptorn visade på en stor minskning, med en uppvisad koncentration som var 41,88% lägre för obesitasgruppen än kontrollgruppen.

Medans det fanns flera intressanta och lovande resultat så hade datan över lag problem med reproducerbarheten, vilket troligtvis stammade från att det enbart gjordes två replikat per grupp. Så framtida arbete borde först och främst fokusera på att utöka mängden data som finns tillgänglig för att ge mer pålitliga resultat innan fokus läggs på andra aspekter.

Acknowledgements

I would first of all like to sincerely thank my supervisor, Lars Nilsson, for supporting and guiding me throughout this entire project and providing me with this opportunity. It was really enjoyable and interesting to work with you, and without your help I would not have been able to accomplish anything even close to what was done in this experiment.

I also want to give a big thanks to Hans Bolinsson for helping me with a large part of my practical work. You taught me how everything worked and made such a large effort to help me get started, and also when things did not go as planned, which it seemed to seldom do during any and every part of the experiment.

I would like to thank Anna-Maria Börjesdotter for providing the protocols used for all parts of the experiment, which made my life a lot easier, especially in the beginning. And thanks to Stephen Burleigh for helping me start to untangle and interpret the data used for my results when I didn't even know where to begin.

And finally I want to thank Novo Nordisk for providing the samples and material used in this project, as well as performing critical analysis of my samples at their facilities. Without this collaboration it would not even have been physically possible to do this experiment in the first place. I want to especially thank Sarah Hyllekvist Jörgensen who put in a lot of time i order to prepare the MS data and present it to me in a nice and easily interpretable format, without which I would probably not have a result at all.

Contents

1 Aims **1**

2 Theory **3**
2.1 Protein Corona . . . 3
2.2 AF4 . . . 3
2.2.1 Membrane . . . 4
2.2.2 Flow . . . 4
2.2.3 Spacer . . . 5
2.2.4 Dispersion Inlet . . . 5
2.2.5 Dilution Control Module . . . 6
2.2.6 Multi Angle Light Scattering . . . 6
2.2.7 UV . . . 6
2.2.8 Differential refractive Index . . . 7
2.3 Mass Spectrometry . . . 7

3 Materials & Methods **9**
3.1 Materials . . . 9
3.2 Methods . . . 9
3.2.1 Preparation of plasma solution & incubation . . . 9
3.2.2 Fractionation using AF4 . . . 9
3.2.3 Lysis, buffer exchange, and digestion . . . 10
3.2.4 Peptide recovery . . . 10
3.2.5 Evotip preparation . . . 10
3.2.6 Mass spectrometry . . . 11

4 Results **13**

5 Discussion **21**

6 Conclusions **23**

7 Future Work **25**

8 Ethics **27**

9 References **29**

10 Appendix **35**
10.1 Figures . . . 35

1 Aims

This thesis will investigate whether obesity can potentially causes a difference in the protein corona formation around lipid nanoparticles in the blood plasma of the treated individual. And if this turns out to be the case, then the goal is also to try and figure out what sort of difference it could make. This aims to improve the understanding of how this increasingly common disease [1], [2] could potentially affect the delivery and efficacy of nanoparticle-based drugs in the treated individuals.

The experiments in this study will be done using plasma from rats, but the goal is for the results to potentially serve as a starting point for further research, eventually including human plasma studies as well.

2 Theory

2.1 Protein Corona

The blood contains a lot of different things; water, cells, proteins, oxygen, carbon dioxide, nutrients, and a lot of other particles/substances. Over 50% of the blood is plasma, which in turn is around 90% water and 10% solutes [3], [4]. A large majority of these solutes are proteins.

Nanoparticles (NPs) are, as the name suggests, particles at the nanometer scale. They where first shown to be of use in biomedicine in the 1970's [5] and have since been proven to be effective drug carriers, being designable to have great target specificity and a controlled release of the cargo [6]. They have even been shown to be able to specifically target tumour cells [7]. However, it's not just as simple as administering a NP-based drug and everything works according to plan. NPs can interact with proteins in the blood so that what is called a "protein corona" is formed around the NP [8]. This affects the behaviour and function of the NP-based drug, but an interesting and also potentially challenging aspect is that this can be both positive and negative [8], [9], [10]. The formation of the protein corona can, depending on the proteins in the corona, cause the drug to be preemtively cleared from the system or cause it to not reach its intended target [10].

To combat these effects, one attempted solution has been to PEGylate the NPs, which is to modify the NPs with polyethylene glycol (PEG) chains. This hinders the binding of proteins that could trigger an immune response and reduces the clearance of the drug [11], [12], [13]. But in a study by Schöttler et al. [9], their results proposed that certain plasma proteins actually need to adhere to the NPs for this effect to happen, as the PEGylated NPs exposed to plasma proteins showed a more specific uptake than those that were not.

One particular group of plasma proteins that are of potential interest is apolipoproteins. They are an important component of lipoproteins, which transport lipids like cholesterol through the body. The apolipoproteins are needed for receptors to recognise the lipoprotein-lipid complexes [14], and so they are the determining factor for where in the body the lipids end up. The apolipoproteins are divided into different classes based on their function. These are Apolipoprotein A, B, C, D, E, F, G, H, J, L, M (ApoA, ApoB, etc.). Among them, all but ApoB can readily dissociate from a lipoprotein and bind to another [15], allowing them to transport several lipids. And so, if the apolipoproteins determine where the lipids go, then if they are part of the protein corona around a nanoparticle they will probably influence where it ends up as well. An apolipoprotein whose interactions with lipid nanoparticles (LNP) have been studied is ApoE. It has been shown that the binding of ApoE to LNPs lead to the particles being transported to and accumulating in the liver [16], [17], affecting the clearance of the drug. This can once again be a boon or a bane depending on the intention/purpose of the administered drug. If the drug is supposed to be delivered to hepatocytes, then this is certainly helpful [18], but if the intended target is outside of the liver, then it would not be preferable to have ApoE bind to the particles. It has been found that other lipoproteins also bind to LNPs [17], making them interesting as well in the scope of this study. Although, they do not have the same effect on hepatic delivery as ApoE [17], and so they should not have as great of an effect on the drug clearance.

2.2 AF4

Asymmetric flow field-flow fractionation (AF4) is a separation technique used to characterise particles in a fluid/solution. The separation is achieved by sending the sample through a fluid-filled channel consisting of several components. The channel consists of two halves: a top half where different

ports are located, and a bottom half where a semi-permeable membrane lays on a frit. These halves are bolted together, separated by a spacer. On the top is an inlet where the carrier fluid used in the system is pumped into the channel, an injection port where the sample is injected into the channel, and an outlet where the sample and carrier fluid exits the channel [19]. In the bottom half is a semi-permeable membrane, supported by a frit. An illustration of a channel can be seen in Figure 2.1

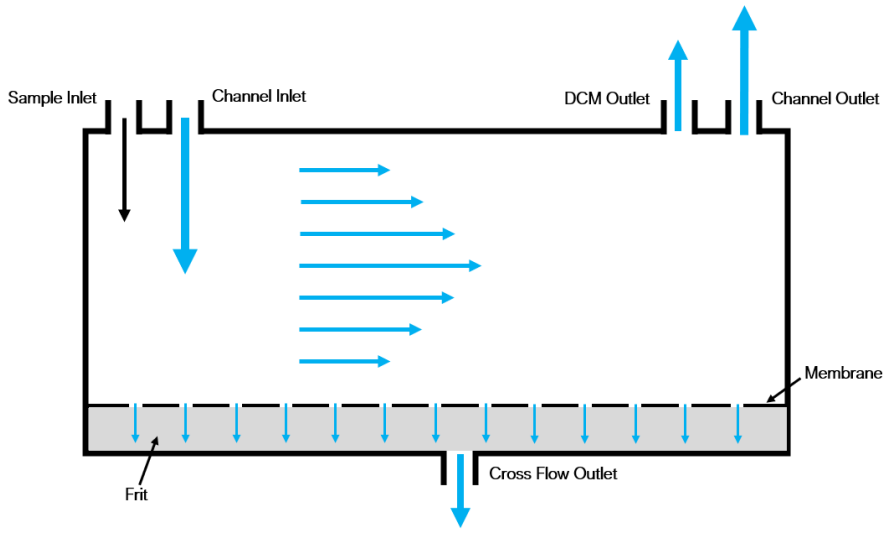

Figure 2.1: Illustration of an AF4 channel with flows indicated by arrows.

2.2.1 Membrane

The membrane's purpose is to keep the analytes in the channel, but letting smaller and unwanted particles pass through. This is achieved by selecting a membrane with a molecular-weight cut-off (MWCO) that is high enough to get rid of the unwanted particles, but keep the analytes. The MWCO determines the smallest particle size that is retained in the channel, letting everything smaller pass through [20].

2.2.2 Flow

In the channel there is a flow from the inlet side towards the outlet side. There is also a cross flow applied to the channel that is perpendicular to the channel flow. This forces the carrier fluid through the semi-permeable membrane at the bottom, carrying the sample particles with it towards the bottom of the channel. The particles smaller than the MWCO also pass through the membrane, and the larger particles stay in the channel [20]. For the particles in the channel, diffusion works in the opposite direction and makes them move up in the channel. Smaller particles diffuse more than large particles, which can be explained with the Stokes-Einstein-Sutherlarnd equation (equation 1)

$$D = \frac{k_B T}{6\pi\eta R_{eff}} \tag{1}$$

D is the diffusion coefficient, k_B is the Boltzmann constant, T is the temperature in kelvin, η is the viscosity of the used solvent, and R_{eff} is the effective or hydrodynamic radius [21]. In the case of AF4, T and η are the same for all particles, so it can be seen from the equation that $D \propto \frac{1}{R_{eff}}$. This tells us what was previously stated; that small particles give a large diffusion coefficient and thus diffuse further in the channel than large particles.

To fully understand how the separation of sample particles work, we also need to look at the flow profile. An important variable here is the Reynolds number which is defined as:

$$Re = \frac{\rho v L_{char}}{\eta} \tag{2}$$

ρ is the density of the fluid, v is the fluid velocity, and L_{char} is a characteristic length (in this case the channel thickness) [22], [23]. The Reynolds number describes the relation between the viscous and inertial forces in a fluid. A large Reynolds number means a high relative inertial force, and so a small number means a high relative viscous force [24], [25]. Considering the variables defining the Reynolds number in an AF4 channel, the fluid velocity and characteristic length will be very small, giving us a small Reynolds number. So the dominating force in an AF4 channel will be viscous. This means that the fluids viscous force is able to compensate the inertial force, keeping the flow aligned. This is what is called a laminar flow [25]. Laminar flow is characterised by having a parabolic flow profile with the fluid velocity increasing from the edges towards the centre of the flow [26]. This is due to the no-slip boundary condition that applies for any viscous fluid in contact with a solid boundary [22]. The condition states that a fluid layer in direct contact with said boundary has no velocity. Then, as there are adjacent fluid layers with differing velocities, viscous shear stress is created between them [27], slightly reducing the velocity of the faster layer and slightly increasing the velocity of the slower (or in this case stagnant) layer [28]. This shear stress spreads through all the layers, creating the mentioned parabolic flow profile. It may be important to mention that the no-slip condition and viscous shear stress is still present in turbulent flow [29], but eddies created in the turbulent flow causes fluid to mix between layers [30] and creating a flat flow profile. Coupling together the facts that small particles diffuse further and that the fluid velocity is higher towards the centre of the channel, we get a system where the smallest particles elute first, with the following particles being in ascending size.

2.2.3 Spacer

As stated previously, the membrane at the bottom of the channel is semi-permeable and lets the carrier fluid through, as otherwise there could not be a cross flow. This means that the amount of carrier fluid in the channel decreases towards the outlet. For a symmetrical channel this would also mean a decreasing fluid velocity towards the outlet [31], which would affect the resolution of the separation. To counteract this, AF4 uses an asymmetrical spacer that is tapered towards the outlet, keeping the fluid velocity constant throughout the channel [31], [32]. The spacer also determines the thickness of the channel, which affects the flow rate profile and resolution [33].

2.2.4 Dispersion Inlet

In order to get a precise size distribution, the injected sample needs to be focused in the channel before the separation begins. In a conventional AF4 channel, the sample is focused by applying two opposite flows to focus the sample in a line close to the membrane. Together with the cross flow, a size-dependent concentration gradient is created [34]. But using this method, proteins and lipid nanoparticles could potentially aggregate or interact with the membrane [34], [35], leading to misleading data and lower mass recovery.

To decrease the probability of this happening, one solution is to use a dispersion inlet channel. This uses hydrodynamic relaxation instead of the two opposing flows to focus the sample, lessening the side effects caused by conventional focusing [34], [35].

2.2.5 Dilution Control Module

Sometimes there could be a problem with the analyte that you are interested in having too low concentration to get a good signal. It could for example be due to the analyte of interest being at a low concentration in the sample, and injecting too much sample could overload the channel, causing increased retention and changing the signal profile [36]. There could also be a low concentration due to there being a limited amount of the sample. One thing that can improve the concentration of a sample is to use a channel with a dilution control module (DCM). The DCM increases the concentration of the sample exiting through the channel outlet by removing some of the carrier fluid at the top of the channel [37]. This works to increase the sample concentration as the particles will be closer to the bottom of the channel due to the applied cross flow, so the removed carrier fluid will contain little to no particles.

2.2.6 Multi Angle Light Scattering

Multi angle light scattering (MALS) analysis is commonly performed together with AF4, getting the molar mass, size, and potentially even the concentration, by shining a laser through the sample and measuring the intensity of the scattered light [38].

When the laser light shines on the macromolecules, the oscillating electric field of the light induces an oscillating dipole in the macromolecules [39]. This dipole will re-emit light with an intensity dependent on how polarised it is, with a greater polarisation leading to a higher intensity [38]. As macromolecules containing more electrons are more polarisable than those with less, the intensity of the scattered light increases with more electrons. In turn, as molecules with more electrons are generally heavier than those with less, the scattered light intensity increases with molar mass.

For MALS analysis there are several detectors, placed at specific angles in relation to the direction of the laser. The intensity of the scattered light measured at these angles from the original direction of the laser can then be used to get the root mean square radius of the macromolecule [38].

The particle concentration for nanoparticles can be determined, given that the volume of the particles, the particles' refractive index, the carrier fluid's refractive index, and the shape of the particles (e.g. sphere or rod) is known [38]. This is entered into the used data collection program (e.g. Astra) to get a calculation of the concentration.

2.2.7 UV

AF4 analysis may also be connected with an on-line UV detection system to get real-time concentration data. A light is shined through the sample stream and a photodetector measures how much light of a certain wavelength is absorbed [40]. Light travelling through a solution follows the Beer-Lambert law:

$$A = \epsilon l c \tag{3}$$

A is the absorbance, ϵ is the molar absorption coefficient, l is the distance the light travels through the solution, and c is the concentration of the solution. So the absorbance is proportional to the concentration of the solution, given that the two other variables are constant. However, the molar absorption coefficient is an intrinsic property of particles, describing how strongly they absorb light from a specific wavelength [41]. As this coefficient can vary between proteins, the UV signal does not provide

an exact concentration. But coupling it together with an RI detector can help create a better picture of the actual concentration.

2.2.8 Differential refractive Index

A differential refractive index (dRI) detector is, as mentioned, used to measure the concentration of analytes in the solvent flowing through it. It has two cells that contain solvent: a reference cell containing the pure solvent, and a sample cell through which the analyte-containing solvent flows [42], [43]. Light is shined through both cells and is then detected by a light sensitive element. When the sample cell only contains pure solvent, the refractive index of the two cells are the same, and so the light refracts the same. But, when analytes enter the sample cell, the refractive index changes, the light refracts at a different angle, and the light sensitive element detects this difference [42], [43]. This difference is proportional to the concentration of analytes in the solvent [44], [43]. This detector is useful in a lot of applications as it can detect any type of analyte in the solvent [42].

2.3 Mass Spectrometry

Mass spectrometry is an analytical technique to help determine the composition of a sample through the measurement of ions' mass-to-charge ratios [45]. An MS-setup consists of three main parts/areas: the ion source, the mass analyser, and the detector [46]. The exact components in each of these parts can differ as there are several ionisation methods, mass analysers, and detectors, but the core function is the same. A simple illustration of an MS-setup can be seen in Figure 2.2.

To begin with, the sample needs to be ionised, and with some methods also fragmented. This can involve energising the sample so that it turns into a gas, or spraying it as a vapour in an applied electric field [46]. The ions are then repelled or propelled into the mass analyser where the ions are sorted. There are several means of sorting/separating the ions. Here, a method using magnetic forces will be explained, but the principle for sorting is similar with other methods, with some exceptions.

After the sample is ionised, the ions pass several accelerating plates with increasingly negative potential, giving the ions kinetic energy relative to their charge and the potential difference the ions pass through. So the kinetic energy of each ion can be expressed as:

$$\frac{mv^2}{2} = zeV \tag{4}$$

m is the mass of the ion, v is its velocity, z is the number of charges of the ion, e is the charge of an electron, and V is the difference in voltage the ions pass [46]. The ions then enter a curved section where a magnetic field is applied. The ions then have two forces acting on them: the magnetic force that is bending the ion towards the centre of the curve, and the centripetal force bending it outwards. For the ion to follow the curve and not end up crashing into the inner or outer wall, the centripetal force needs to exactly counteract the magnetic force. So the relationship can be written like in equation 5.

$$\frac{mv^2}{r} = Bzev \tag{5}$$

r is the circular radius of the curved segment, and B is the magnetic field strength [46], [47], [48]. This can then be rearranged to get an expression for v^2 as follows

$$v^2 = (\frac{Bzer}{m})^2 \tag{6}$$

If equation 4 is rearranged with v^2 on one side, it can then be substituted into equation 6 to get

$$\frac{2zeV}{m} = (\frac{Bzer}{m})^2 \tag{7}$$

Rearranging it once more, an expression for $\frac{m}{z}$ is found

$$\frac{m}{z} = \frac{(Br)^2 e}{2V} \tag{8}$$

So, as B, r, and V is given, only ions with a specific mass-to-charge ratio can pass through the curve and reach the detector [46]. Ions with a higher $\frac{m}{z}$ would crash into the outer wall, and ions with lower $\frac{m}{z}$ would crash into the inner wall. The voltage in the accelerating plates and/or the magnetic force can then be changed to allow ions of differing mass-to-charge ratios to be detected [46]. The result is then a graph with peaks corresponding to the peptides in the sample, with the $\frac{m}{z}$-values on the x-axis and the relative intensity on the y-axis.

To get even more information about the sample, tandem MS (MS/MS) can be used. This involves choosing ions from the first separation, fragmenting them, and then performing another separation [49]. This provides information about the structure of the chosen ions and can help distinguish between ions with the same or very similar mass-to-charge ratios.

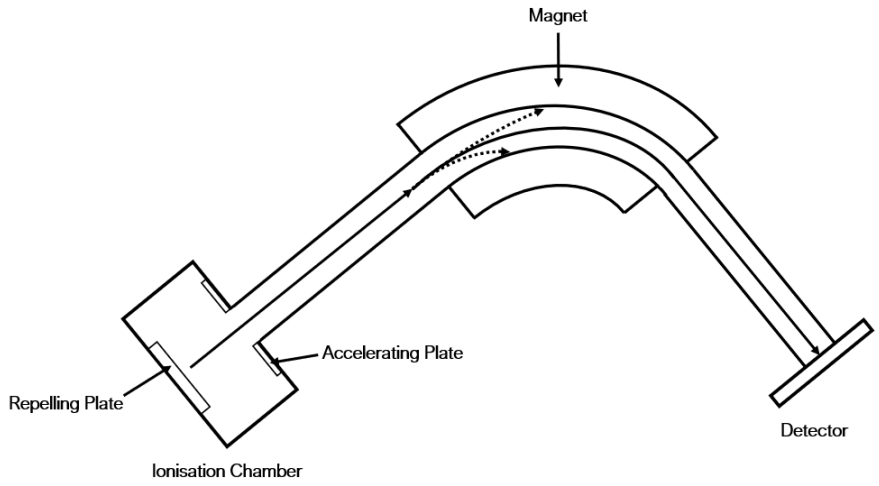

Figure 2.2: Simple example of a Mass Spectrometric setup. An ionisation chamber with a repelling plate and accelerating plates, a curved section with a surrounding magnet, and a detector. The solid arrows show the path of ions that have a mass-to-charge ratio so that their centripetal force exactly counteracts the magnetic force from the magnet. The dotted arrows show the path of ions that do not have this mass-to-charge ratio.

3 Materials & Methods

3.1 Materials

The carrier used for the AF4 was prepared using sodium chloride (prod. no 27810.295, VWR), unprotonated tris(hydroxymethyl)aminomethane (prod. no. 108382, Merck), sodium azide (prod. no. S2002-100G, Merck), hydrochloric acid (prod. no. 30018.298, VWR), and Milli-Q water. For the lysis buffer, guanidine (prod. no. G7294-100ML, Sigma-Aldrich), tris(2-carboxyethyl)phosphine (prod. no. 77720, Thermo Scientific), and 2-chloroacetamide was used (prod. no. C0267-100G, Sigma-Aldrich). The digest buffer was prepared using tetraethylammonium bicarbonate buffer (prod. no. T7408-100ML, Sigma-Aldrich). Trypsin solution was prepared with lyophilised trypsin/Lys-C mix (prod. no. V5071, Promega) and digest buffer.

Solvent A used in the Evotip preparation contained 0.1% formic acid (prod. no. 84865.290, VWR), and solvent B contained 0.1% formic acid in acetonitrile (prod. no. 100029, Supelco).

The LNPs provided by Novo Nordisk where at a concentration of 0.1 mg/mL.

3.2 Methods

3.2.1 Preparation of plasma solution & incubation

The plasma was obtained from Novo Nordisk as samples from individual rats. The plasma was pooled into two groups: control and obese, containing plasma in equal volumes from three and six individuals respectively. Pooled plasma was then added to LNPs in a ratio of 2.9 μl plasma per 100 μl LNP. Every sample was incubated for one hour at 37^oC in an Eppendorf ThermoMixer C.

3.2.2 Fractionation using AF4

The fractionation using AF4 was done with an Eclipse NEON WEC-04 system (Wyatt Technology) connected to a chromatographic system. The chromatographic system contained a degasser (model 2003, Biotech), QuatPump (G1311A, Agilent Technologies), autosampler (G1313A, Agilent), MALS detector (DAWN HELEOS-II, Wyatt), dRI detector (Optilab T-rEX, Wyatt), diode array detector (G1315A, Hewlett Packard & Agilent), and fraction collector (G1364F, Agilent). The setup can be seen in Figure 3.1 The system was controlled using the Vision Run software (Wyatt) and the data was collected with Astra (Wyatt).

The fractionation was performed at room temperature with an Eclipce dispersion inlet channel (Wyatt) with a 275 μm spacer and 10 kDa cut-off regenerated cellulose membrane. The carrier contained 25 mM tris(hydroxymethyl)aminomethane, 50 mM sodium chloride, and 0.02% sodium azide. The pH of the carrier was adjusted to 7.4 with 5 M HCL. The separation method was 35 minutes long, with a cross flow of 2.00 ml/min the first five minutes, then over five minutes it decreased linearly to 0.30 ml/min, followed by a 20 minute linear decrease to 0.05 ml/min, and then five minutes with no cross flow. The channel flow was set to 1.75 ml/min, and both the inject flow and detector flow was set to 0.20 ml/min. The injected sample volume was 250 μl. Two injections were measured and fractionated for each plasma group, doing a total of four. The collected fractions were put in a refrigerator at 4 ^oC over night. The first attempted fractionation for the control group was not used as there was a suspected concentration difference compared to supposed concentration, and the UV detector stopped working part-way through. So a third fractionation for the control group was performed the day after. The injections for the control group will thus be labelled ”Control 2” and ”Control 3” in

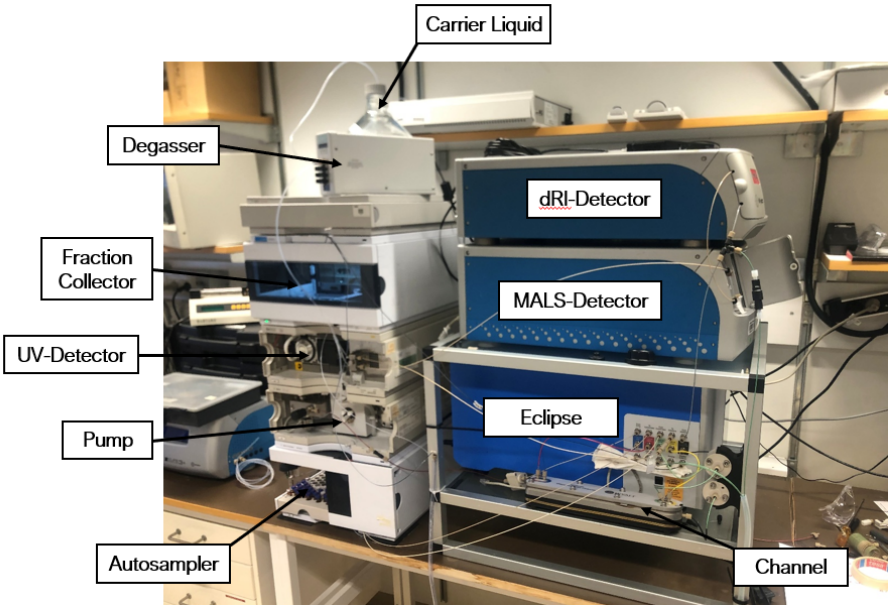

Figure 3.1: Setup used during experiment with labelled components.

this report. Five fractions from each injection, corresponding to the protein-LNP peaks, were used in the continued experiment.

3.2.3 Lysis, buffer exchange, and digestion

For each fraction, 100 μl was transferred to a 1.5 ml eppendorf tube, then adding 100 μl lysis buffer. All the tubes were then placed in an Eppendorf ThermoMixer C for ten minutes at 90 ^oC and 900 rpm, then let to cool down to room temperature. 100 μl from each tube was then transferred to Vivacon 10 kDa spin filters with collection tubes. They were then spun at 10,000 g in an Eppendorf MiniSpin for a total of 20 minutes so that all liquid had gone through the filter, and the flowthrough was discarded. Repeating once, 100 μl of digest buffer was added and the tubes were then again spun at 10,000 g for 20 minutes, discarding the flowthrough. The collection tubes were exchanged for new ones and 50 μl digest buffer were added to the filters. The trypsin solution was prepared by adding 400 μl digest buffer to a vial of 20 μg lyophilised trypsin/Lys-C mix, then 20 μl was added to the filters. They were then incubated overnight in the ThermoMixer at 37 ^oC and 750 rpm.

3.2.4 Peptide recovery

The following day, the tubes and filters were spun at 10,000 g in the MiniSpin for 15 minutes. 50 μl of 25 mM NaCl solution was added to the filters and then spun at 10,000 g in the MiniSpin for 15 minutes so that all liquid had gone through the filter. The filters were discarded and the flowthrough was collected, and 15 μl of 1% TFA was added to the collection tubes.

3.2.5 Evotip preparation

One Evotip per fraction was placed in a 96-tip Evotip box. 20 μl of solvent B was added to each tip and the box was spun at 800 g in an Eppendorf centrifuge (model 5805R, with A-2-DWP rotor) for 60 seconds. The solvent in the box was discarded and isopropanol was poured in the bottom of the box so the bottom of the tips were covered. They were let to soak until the loaded tips were a pale white, then the isopropanol was discarded. 20 μl of solvent A was added to each tip and the box was spun

at 800 g in the Eppendorf centrifuge for 60 seconds. The solvent in the box was discarded and 100 μl of the samples were loaded in their corresponding tip, then the box was spun at 800 g in Eppendorf centrifuge for 60 seconds. The flowthrough was discarded and 60 μl of solvent A was added to each tip, then the box was spun at 800 g in the Eppendorf centrifuge for 180 seconds. The flowthrough was discarded and 100 μl of solvent A was added to each tip and the box was spun at 800 g in the Eppendorf centrifuge for 10 seconds, just so the solvent soaks the loaded tip but does not run through. Each tip was transferred to individual 3.6 ml cryogenic vials with screw caps (Thermo Scientific) and placed in a refrigerator at 4 ^oC. The day after, a bit of solvent A was added to the bottom of each tube to make sure the tips don't dry out.

3.2.6 Mass spectrometry

The mass spectrometric analysis was performed by Novo Nordisk at their facility in Måløv. They collected the prepared Evotips the day after being put in the fridge and performed LC-MS/MS analysis the following week.

4 Results

The data collected from the AF4 separation can bee seen in Figures 4.1-4.4. There, the light scattering, dRI, UV, molar mass, and RMS radius data can be seen. Channel and flow data can also be seen in Figures 4.5-4.10, including channel pressure, inlet flow, read channel flow, read cross flow, read detector flow, and read inject flow. These graphs show the data from all of the injections in the same plot. The plots with the individual data can be found in the Appendix.

From the MS analysis, 999 different proteins were detected. Due to this extensive amount of data combined with the limited time available to analyse it, the presented results will only include the apolipoproteins and certain proteins identified by Novo Nordisk to be of interest. It will also be limited to those of these proteins that did not have any blank/missing values for any fraction. Something important to note is that the values from the second fraction for the first obese injection was set as the average for that injection per protein. The raw MS data for the control and obese injections can be found in Table 4.1 and Table 4.2 respectively. The coefficient of variation (CV) between the two replicates within a group for each protein can be found in Table 4.3, and the percentual difference between the two groups' averages can be found in Table 4.4.

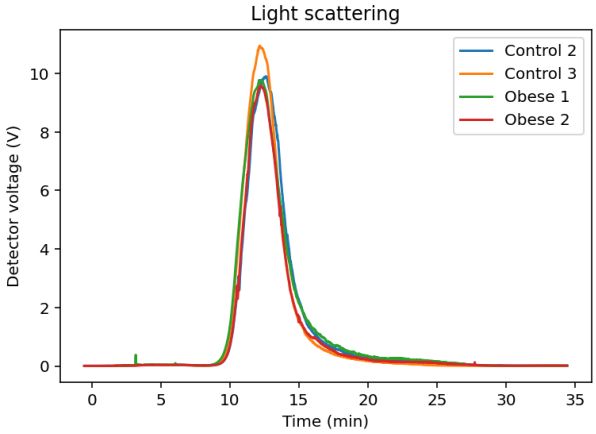

Figure 4.1: Light scattering at a 90^o angle from the incident beam for all injections throughout the separation process.

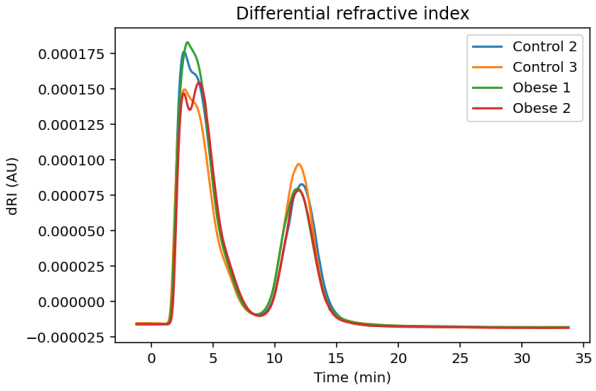

Figure 4.2: Differential refractive index for all injections throughout the separation process.

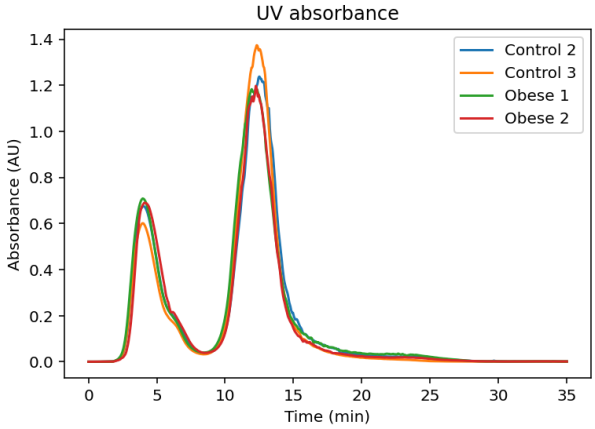

Figure 4.3: UV absorption for all injections throughout the separation process.

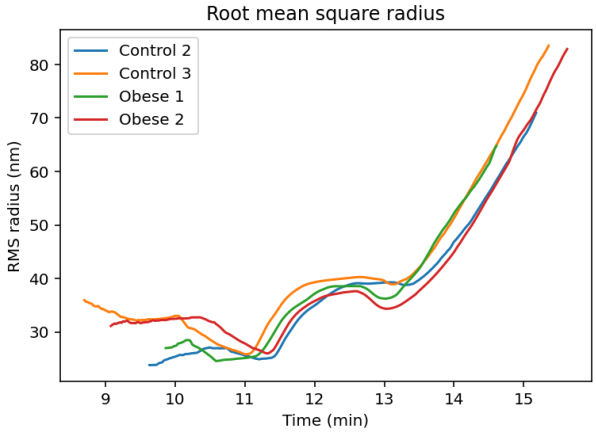

Figure 4.4: Root mean square radius for all injections over the time of the protein peak. The exact length in the x-direction for each injection depends only on the manually placed peak intervals in Astra.

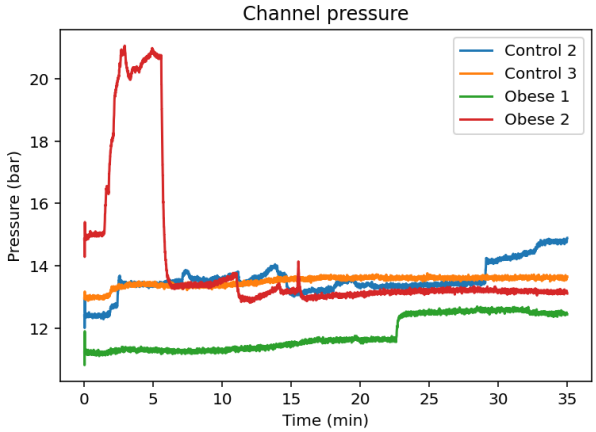

Figure 4.5: Channel pressure for all injections throughout the separation process.

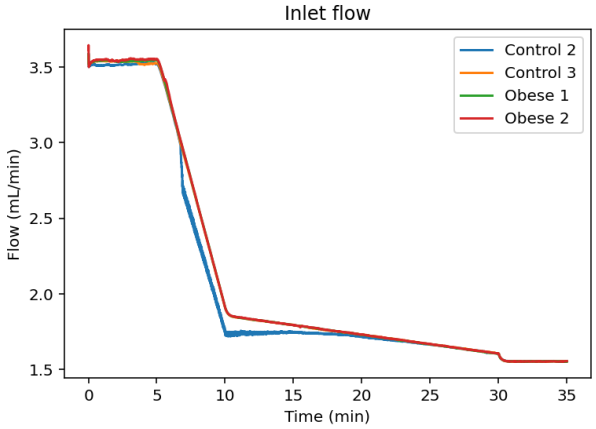

Figure 4.6: Inlet flow for all injections throughout the separation process.

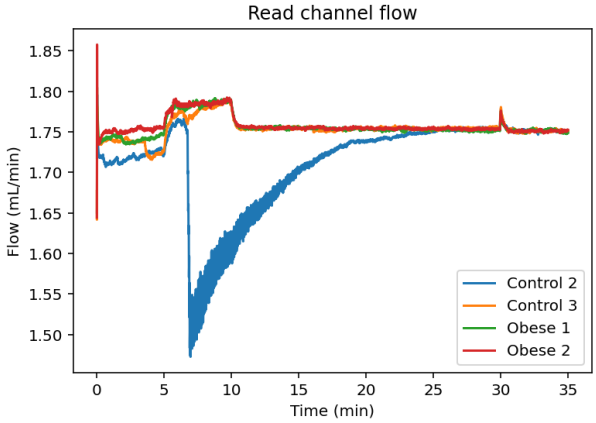

Figure 4.7: Read channel flow for all injections throughout the separation process.

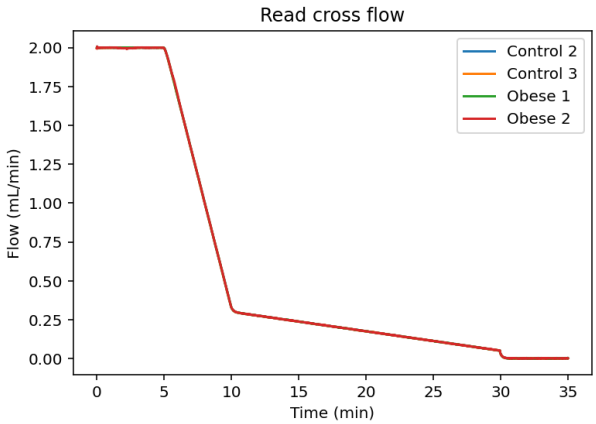

Figure 4.8: Read cross flow for all injections throughout the separation process.

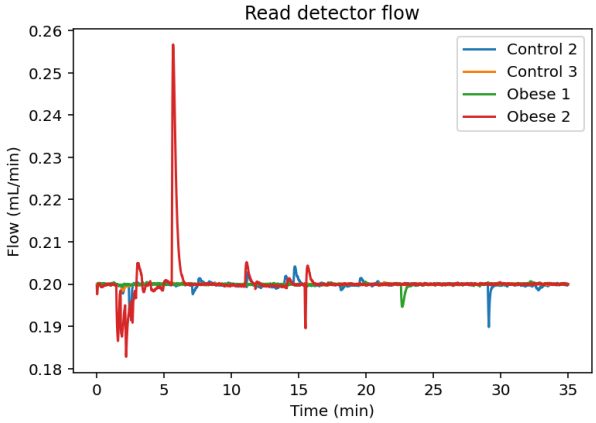

Figure 4.9: Read detector flow for all injections throughout the separation process.

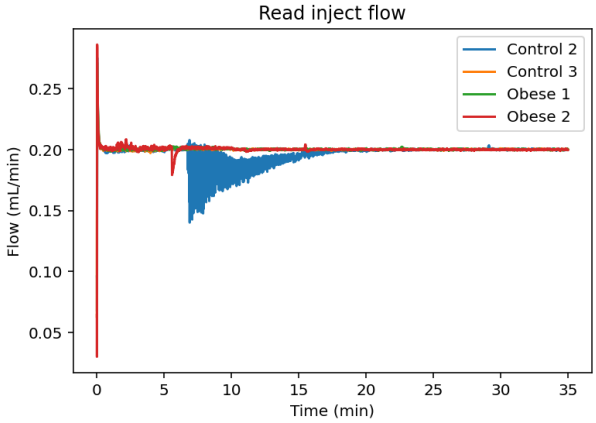

Figure 4.10: Read inject flow for all injections throughout the separation process.

Table 4.1: Number of precursors, injection number, and detected intensity in each fraction (F 1-5) for 17 proteins of interest for the Control group. The number of precursors for a protein can be seen as an indication of how likely it is to be correctly identified, with a higher number meaning more likely. The fractions are each one minute, starting at minute 10 of the injection and ending at minute 15. The intensity values are in $\log_2$.

Control							
Protein	**Precursors**	**Inj.**	**F 1**	**F 2**	**F 3**	**F 4**	**F 5**
Albumin	211	2	16,90	16,27	15,86	15,23	14,77
Apolipoprotein A-I	82	2	14,23	13,87	13,88	13,66	13,63
Apolipoprotein A-II	11	2	15,32	14,91	14,69	13,90	14,29
Apolipoprotein A-IV	106	2	13,25	13,09	13,48	13,97	14,84
Apolipoprotein B-100	132	2	11,47	11,94	12,41	12,59	12,26
Apolipoprotein C-I	12	2	11,28	9,75	9,07	9,75	8,55
Apolipoprotein C-II	14	2	11,67	10,98	11,59	11,38	11,40
Apolipoprotein C-IV	8	2	7,69	6,58	6,45	6,91	7,79
Apolipoprotein E	108	2	15,05	14,18	14,01	13,93	14,06
Beta-2-glycoprotein 1	24	2	9,16	8,96	8,93	9,01	9,28
Apolipoprotein M	10	2	6,58	7,20	7,18	7,14	7,63
Apolipoprotein N	5	2	12,33	10,95	11,62	11,51	11,79
Fibronectin	177	2	13,54	13,97	14,81	15,01	14,33
Ig gamma-2B chain C region	31	2	13,82	14,03	13,40	13,69	13,69
Immunoglobulin heavy constant mu	46	2	14,64	14,93	15,84	15,97	16,20
Immunoglobulin joining chain	9	2	8,21	8,77	10,06	11,25	11,01
Polymeric immunoglobulin receptor	7	2	7,89	7,90	8,79	8,95	9,12
Albumin	211	3	16,48	15,98	16,01	15,66	14,93
Apolipoprotein A-I	82	3	13,74	13,32	14,00	14,20	13,84
Apolipoprotein A-II	11	3	15,17	14,75	14,47	14,54	14,18
Apolipoprotein A-IV	106	3	12,84	13,49	13,87	14,75	15,27
Apolipoprotein B-100	132	3	10,65	11,89	12,50	12,02	12,01
Apolipoprotein C-I	12	3	11,01	8,29	9,60	12,70	8,64
Apolipoprotein C-II	14	3	10,37	9,87	11,34	11,56	11,45
Apolipoprotein C-IV	8	3	6,98	7,94	6,38	7,09	7,62
Apolipoprotein E	108	3	14,26	13,43	14,18	14,62	14,63
Beta-2-glycoprotein 1	24	3	8,56	8,65	8,99	8,94	9,32
Apolipoprotein M	10	3	7,68	7,46	7,21	7,07	7,74
Apolipoprotein N	5	3	11,19	10,31	10,97	12,11	11,72
Fibronectin	177	3	13,66	14,09	14,74	14,52	14,61
Ig gamma-2B chain C region	31	3	13,84	13,66	13,68	13,56	13,27
Immunoglobulin heavy constant mu	46	3	14,07	14,35	15,77	16,06	16,24
Immunoglobulin joining chain	9	3	6,98	8,88	9,84	10,94	10,83
Polymeric immunoglobulin receptor	7	3	7,03	7,67	9,19	8,89	9,00

Table 4.2: Number of precursors, injection number, and detected intensity in each fraction (F 1-5) for 17 proteins of interest for the obese group. The number of precursors for a protein can be seen as an indication of how likely it is to be correctly identified, with a higher number meaning more likely. The fractions are each one minute, starting at minute 10 of the injection and ending at minute 15. The intensity values are in $\log_2$.

Obese							
Protein	**Precursors**	**Inj.**	**F 1**	**F 2**	**F 3**	**F 4**	**F 5**
Albumin	211	1	17,04	15,89	15,68	15,40	15,44
Apolipoprotein A-I	82	1	14,17	13,70	13,18	13,64	13,83
Apolipoprotein A-II	11	1	15,48	14,83	14,30	14,81	14,71
Apolipoprotein A-IV	106	1	13,42	14,43	13,99	14,61	15,70
Apolipoprotein B-100	132	1	11,08	11,90	12,47	12,49	11,58
Apolipoprotein C-I	12	1	14,00	11,44	9,00	8,85	13,93
Apolipoprotein C-II	14	1	10,65	11,07	12,34	11,26	10,01
Apolipoprotein C-IV	8	1	9,16	7,99	7,65	7,46	7,70
Apolipoprotein E	108	1	15,09	14,25	13,48	13,91	14,53
Beta-2-glycoprotein 1	24	1	9,69	9,24	8,83	9,31	9,13
Apolipoprotein M	10	1	6,93	6,55	6,21	7,13	5,92
Apolipoprotein N	5	1	13,02	12,14	11,84	11,26	12,43
Fibronectin	177	1	13,77	14,28	14,82	14,57	13,98
Ig gamma-2B chain C region	31	1	13,84	13,19	13,20	12,91	12,83
Immunoglobulin heavy constant mu	46	1	14,97	15,58	15,35	15,94	16,05
Immunoglobulin joining chain	9	1	8,35	9,64	9,11	10,22	10,90
Polymeric immunoglobulin receptor	7	1	6,33	7,62	7,42	8,81	7,92
Albumin	211	2	16,64	16,91	16,01	15,29	15,23
Apolipoprotein A-I	82	2	14,10	14,41	14,01	13,70	14,07
Apolipoprotein A-II	11	2	15,92	15,86	14,72	14,74	14,69
Apolipoprotein A-IV	106	2	13,04	13,83	14,08	14,67	15,49
Apolipoprotein B-100	132	2	11,13	11,71	12,66	12,45	12,19
Apolipoprotein C-I	12	2	13,82	13,15	9,84	8,12	10,63
Apolipoprotein C-II	14	2	12,47	11,61	10,94	11,90	11,39
Apolipoprotein C-IV	8	2	8,39	9,16	6,81	7,57	7,62
Apolipoprotein E	108	2	14,95	14,79	13,85	13,89	14,35
Beta-2-glycoprotein 1	24	2	8,09	8,77	9,10	8,98	9,69
Apolipoprotein M	10	2	6,31	7,01	6,92	7,40	7,44
Apolipoprotein N	5	2	11,11	11,72	11,40	10,55	10,87
Fibronectin	177	2	14,85	14,03	14,65	14,59	14,16
Ig gamma-2B chain C region	31	2	14,77	13,57	13,63	13,20	13,24
Immunoglobulin heavy constant mu	46	2	16,98	15,11	15,62	15,71	15,92
Immunoglobulin joining chain	9	2	9,08	9,47	9,32	10,15	10,96
Polymeric immunoglobulin receptor	7	2	6,15	7,29	8,17	8,36	8,07

Table 4.3: Coefficient of variation (CV) for every protein of interest for each groups separately.

Protein	CV, C (%)	CV, O (%)
Albumin	5,07	6,83
Apolipoprotein A-I	1,08	16,50
Apolipoprotein A-II	2,08	20,84
Apolipoprotein A-IV	20,52	8,75
Apolipoprotein B-100	12,66	6,16
Apolipoprotein C-I	46,94	21,24
Apolipoprotein C-II	17,56	23,22
Apolipoprotein C-IV	5,42	0,27
Apolipoprotein E	1,29	3,90
Beta-2-glycoprotein 1	7,73	12,28
Apolipoprotein M	13,14	22,09
Apolipoprotein N	15,63	50,15
Fibronectin	2,74	7,55
Ig gamma-2B chain C region	6,13	27,61
Immunoglobulin heavy constant mu	4,30	18,84
Immunoglobulin joining chain	12,20	3,35
Polymeric immunoglobulin receptor	2,28	1,68

Table 4.4: Percentual difference between the averages of the two groups as compared to the average of the control group. A positive value means that there is an increase of that protein in the obese group, and negative means a decrease.

Protein	Average difference between groups (%)
Albumin	11,43
Apolipoprotein A-I	4,07
Apolipoprotein A-II	34,33
Apolipoprotein A-IV	36,29
Apolipoprotein B-100	-0,05
Apolipoprotein C-I	304,92
Apolipoprotein C-II	21,61
Apolipoprotein C-IV	85,34
Apolipoprotein E	6,95
Beta-2-glycoprotein 1	10,76
Apolipoprotein M	-27,55
Apolipoprotein N	19,83
Fibronectin	0,68
Ig gamma-2B chain C region	-8,33
Immunoglobulin heavy constant mu	18,30
Immunoglobulin joining chain	-15,52
Polymeric immunoglobulin receptor	-41,88

5 Discussion

The results show that there is something that is causing a non-negligible change in several of the proteins of interest across between the two groups. Looking at the average difference between groups (Table 4.4), most of the proteins seem to show an increased presence in the protein corona in the obese group. But when simultaneously looking at the CVs [50] and number of precursors for the proteins as well, it should probably be deduced that the average difference alone is not entirely a perfect representation of the actual changes in protein presence due to obesity.

The value that stands out the most among the average differences is for Apolipoprotein C-I, which shows a supposed increase of 304,92%. But checking its CV values, it can be seen that both the control group and obese group shows significantly high variation. This means that there is a large variation between the two replicates in the same group. So the result might be due to some error in the preparation/handling, some random variation in the two samples, or some irregularity during the separation process. It can for example bee seen in Figure 4.5 that the second obese injection had vastly increased channel pressure for several minutes, and in Figure 4.7 the first obese injection is shown to have a decreased channel flow for a substantial part of the separation process. But several proteins showed quite small CV values in both groups, so it is not entirely clear what the precise cause is.

Several other large differences could also potentially be explained with similar reasoning. Apolipoprotein A-II has a large CV for the obese group, but okay amounts of precursors; Apolipoprotein A-IV has a large CV for the control group, although a large amount of precursors; Apolipoprotein C-II has large CVs for both groups, but okay amounts of precursors; Apolipoprotein M has high CVs, but okay precursor amounts; Apolipoprotein N has very high CVs and potentially few precursors; Immunoglobulin heavy constant mu has a large CV for the obese group, but quite a lot of precursors.

So while a lot of the large average differences could potentially be disregarded with this argumentation, it is not completely black and white. Although CV is a good way to see if an experiment has good reproducibility and can be trusted [50], the amount of precursors is harder to use to come to a definitive answer. The more precursors detected for a protein, the more confident on an identification it is, but it is hard to draw a line of when it is too few to trust the result. Some proteins can also only identifiable from a single precursor, and others can have overlaps, making them harder to correctly identify [51]. But although some of the proteins here have low precursor counts compared to other proteins, they all seem to have a passable amount to not be immediately disregarded [51], [52]. Still, the previously mentioned proteins all have excessively high CV values, and should probably not be completely trusted.

Looking at the remaining proteins, we should start with the albumin. It is included in these proteins mainly to serve as a sort of proof that nothing major is wrong. It is the most abundant plasma protein, accounting for 50-60% of them, and it is also quite small, with a molecular weight of around 66-67kDa [53], [54]. Albumin also has a low binding affinity to nanoparticles compared to other proteins present in blood [55], meaning that it will largely be unbound. This means that it will elute early in the separation process, greatly contributing to the peak at around minute five that can be seen in Figure 4.2 and 4.3. But as can be seen, there is some overlap between the peaks, so some albumin will be present in the fractions from the second peak. And so, if something is not very wrong, the albumin intensity will be decreasing over the five minutes of the analysed fractions. And looking at Table 4.1 and 4.2, that is exactly what can be seen, and the CVs are quite low. So it can from that be concluded that the results should not be entirely incorrect.

Continuing, we have Apolipoprotein A-I with a small increase, although the obese CV is definitely on the higher end, so this could very well be inaccurate; Apilipoprotein B-100 shows almost no change, with passable CVs; Apolipoprotein C-IV with a very large increase, having low CVs; Apolipoprotein E with a small increase and small CVs; Beta-2-glycoprotein 1 with a small increase and passable CVs; Fibronectin with nearly no change, having small CVs; Ig gamma-2B chain C region with a small decrease, but a high obese CV; Immunoglobulin joining chain with a decent decrease and passable CVs; Polymeric immunoglobulin receptor with a large decrease and low CVs.

So, after looking at these last proteins, it can be concluded that there are eight of these proteins that have more trustworthy data than the others: Albumin, Apolipoprotein B-100, Apolipoprotein C-IV, Apolipoprotein E, Beta-2-glycoprotein 1, Fibronectin, Immunoglobulin joining chain, and Polymeric immunoglobulin receptor.

There does not seem to be a lot of similar studies, but one that was found compared the proteins present in the protein corona around gold nanoparticles with two different coatings under healthy and obese conditions [56]. They looked at particles with a diameter of 20 and 100 nm, the latter of which is more relevant for comparison to this present study, as can be seen in Figure 4.4. As far as I understand, the study showed that Apolipoprotein B, C-IV, E, and fribronectin were present at an increased level under obese conditions. The immunoglobulin joining chain and the polymeric immunoglobulin receptor showed decreased presence, the results for beta-2-glycoprotein 1 was mixed, and albumin was not present in the presented data [56]. This does for the most part mirror the results gotten in this study, although I can not say how well the amplitude of these changes match.

It is interesting that the large changes showed in Apolipoprotein C-IV and Polymeric immunoglobulin receptor show such great reproducibility when looking at the CV values. Although, looking at Table 4.1 and 4.2, it can be seen that these two protein's intensity values are not that high as compared to many others in this experiment. So a change in concentration due to any reason would affect the percentage difference greater for these proteins than most of the others. But saying that, they are still very fascinating results assuming they are true.

It should be mentioned and taken into account that there are a few factors that affect the potential validity of the results and the ability to compare it to other studies. Firstly, the experiment in this study was performed on rat plasma, while the cited and most relevant study for these proteins was done on human plasma. Also, the particles used were not the same for this and the cited study, which would likely change the results in some way. And lastly, as briefly mentioned earlier, the amount of individual rats making up each group is quite low. So this could leave room for a difference in one individual to affect the results.

6 Conclusions

The results show some interesting results with good reproducibility across this experiment, some of which differ from results of previous plasma proteomic studies. Most of the more trustworthy data for individual proteins show an increased presence in the protein corona for the obese group, with a couple showing a decrease. Some proteins with very significant and unexpected differences between the groups showed good reproducibility in this experiment. As almost all of the apolipoproteins in this experiment show an increased protein corona presence, it proposes that the delivery of LNP-based drugs would likely be more greatly affected in individuals with obesity.

But it also needs to once again be said that this experiment should not be used to draw any major conclusions, as it has a very small sample size and includes several factors that could possibly skew the results. Instead, it should be seen as an experiment with some potentially interesting results that could be further and more extensively looked into.

7 Future Work

For future work following this experiment, the first priority should be to increase the sample size. Meaning, increasing both the amount of replicates, and the number of individuals that are part of each group, as this would provide more conclusive results. There should also be an expanded proteomic analysis, investigating more protein groups, or as a final goal, the entirety of the identified proteins. Another interesting factor would be to, in addition to the other groups, look at individuals that have been obese and then lost weight, both close in time to the weight loss as well as later on. This could potentially show if becoming obese has any effects on the protein corona formation even after not being obese any more, and then also if these effects are short or long term.

8 Ethics

It is of importance to mention that this experiment would usually not be allowed to be performed due to ethical reasons. The amount of data and results that are obtained from it does not justify the euthanisation of nine rats. However, the plasma samples used were not collected for this experiment. They were instead collected during another experiment performed by Novo Nordisk, for which they have an ethical permit. So the samples in this experiment can be seen as leftover material from another study, operating within the ethical boundaries.

9 References

[1] *Obesity and overweight*. en. URL: https://www.who.int/news-room/fact-sheets/detail/obesity-and-overweight (visited on 07/06/2026).

[2] Chrysi Koliaki, Maria Dalamaga, and Stavros Liatis. "Update on the Obesity Epidemic: After the Sudden Rise, Is the Upward Trajectory Beginning to Flatten?" In: *Current Obesity Reports* 12.4 (2023), pp. 514–527. ISSN: 2162-4968. DOI: 10.1007/s13679-023-00527-y. URL: https://pmc.ncbi.nlm.nih.gov/articles/PMC10748771/ (visited on 07/06/2026).

[3] *Blood Basics*. en. URL: https://www.hematology.org/education/patients/blood-basics (visited on 05/21/2026).

[4] "In brief: What does blood do?" en. In: *InformedHealth.org [Internet]*. Institute for Quality and Efficiency in Health Care (IQWiG), Mar. 2023. URL: https://www.ncbi.nlm.nih.gov/books/NBK279392/ (visited on 05/21/2026).

[5] Obaid Afzal et al. "Nanoparticles in Drug Delivery: From History to Therapeutic Applications". In: *Nanomaterials* 12.24 (Dec. 2022), p. 4494. ISSN: 2079-4991. DOI: 10.3390/nano12244494. URL: https://pmc.ncbi.nlm.nih.gov/articles/PMC9781272/ (visited on 05/21/2026).

[6] Azeez Yusuf et al. "Nanoparticles as Drug Delivery Systems: A Review of the Implication of Nanoparticles' Physicochemical Properties on Responses in Biological Systems". In: *Polymers* 15.7 (Mar. 2023), p. 1596. ISSN: 2073-4360. DOI: 10.3390/polym15071596. URL: https://pmc.ncbi.nlm.nih.gov/articles/PMC10096782/ (visited on 05/21/2026).

[7] Shreelaxmi Gavas, Sameer Quazi, and Tomasz M. Karpiński. "Nanoparticles for Cancer Therapy: Current Progress and Challenges". In: *Nanoscale Research Letters* 16 (Dec. 2021), p. 173. ISSN: 1931-7573. DOI: 10.1186/s11671-021-03628-6. URL: https://pmc.ncbi.nlm.nih.gov/articles/PMC8645667/ (visited on 05/21/2026).

[8] Sung Jean Park. "Protein–Nanoparticle Interaction: Corona Formation and Conformational Changes in Proteins on Nanoparticles". In: *International Journal of Nanomedicine* 15 (Aug. 2020), pp. 5783–5802. ISSN: 1176-9114. DOI: 10.2147/IJN.S254808. URL: https://pmc.ncbi.nlm.nih.gov/articles/PMC7418457/ (visited on 05/21/2026).

[9] Susanne Schöttler et al. "Protein adsorption is required for stealth effect of poly(ethylene glycol)- and poly(phosphoester)-coated nanocarriers". en. In: *Nature Nanotechnology* 11.4 (Apr. 2016), pp. 372–377. ISSN: 1748-3395. DOI: 10.1038/nnano.2015.330. URL: https://www.nature.com/articles/nnano.2015.330 (visited on 05/21/2026).

[10] Elizabeth Voke et al. "Protein corona formed on lipid nanoparticles compromises delivery efficiency of mRNA cargo". en. In: *Nature Communications* 16.1 (Sept. 2025), p. 8699. ISSN: 2041-1723. DOI: 10.1038/s41467-025-63726-2. URL: https://www.nature.com/articles/s41467-025-63726-2 (visited on 02/18/2026).

[11] Steevens N. S. Alconcel, Arnold S. Baas, and Heather D. Maynard. "FDA-approved poly(ethylene glycol)–protein conjugate drugs". en. In: *Polymer Chemistry* 2.7 (June 2011), pp. 1442–1448. ISSN: 1759-9962. DOI: 10.1039/C1PY00034A. URL: https://pubs.rsc.org/en/content/articlelanding/2011/py/c1py00034a (visited on 05/21/2026).

[12] Francesco M. Veronese and Gianfranco Pasut. "PEGylation, successful approach to drug delivery". In: *Drug Discovery Today* 10.21 (Nov. 2005), pp. 1451–1458. ISSN: 1359-6446. DOI: 10.1016/S1359-6446(05)03575-0. URL: https://www.sciencedirect.com/science/article/pii/S1359644605035750 (visited on 05/21/2026).

[13] Sara Zalba et al. “Stealth nanoparticles in oncology: Facing the PEG dilemma”. In: *Journal of Controlled Release* 351 (Nov. 2022), pp. 22–36. ISSN: 0168-3659. DOI: 10.1016/j.jconrel.2022.09.002. URL: https://www.sciencedirect.com/science/article/pii/S0168365922005867 (visited on 05/21/2026).

[14] Zijun Ma et al. “The functions of apolipoproteins and lipoproteins in health and disease”. In: *Molecular Biomedicine* 5 (Oct. 2024), p. 53. ISSN: 2662-8651. DOI: 10.1186/s43556-024-00218-7. URL: https://pmc.ncbi.nlm.nih.gov/articles/PMC11513782/ (visited on 06/05/2026).

[15] Sakeel Ahmed, Abhay H. Pande, and Shyam Sunder Sharma. “Therapeutic potential of ApoE-mimetic peptides in CNS disorders: Current perspective”. In: *Experimental Neurology* 353 (July 2022), p. 114051. ISSN: 0014-4886. DOI: 10.1016/j.expneurol.2022.114051. URL: https://www.sciencedirect.com/science/article/pii/S0014488622000760 (visited on 06/05/2026).

[16] Federica Sebastiani et al. “Apolipoprotein E Binding Drives Structural and Compositional Rearrangement of mRNA-Containing Lipid Nanoparticles”. In: *ACS Nano* 15.4 (Apr. 2021), pp. 6709–6722. ISSN: 1936-0851. DOI: 10.1021/acsnano.0c10064. URL: https://pmc.ncbi.nlm.nih.gov/articles/PMC8155318/ (visited on 06/05/2026).

[17] Akin Akinc et al. “Targeted Delivery of RNAi Therapeutics With Endogenous and Exogenous Ligand-Based Mechanisms”. English. In: *Molecular Therapy* 18.7 (July 2010), pp. 1357–1364. ISSN: 1525-0016, 1525-0024. DOI: 10.1038/mt.2010.85. URL: https://www.cell.com/molecular-therapy-family/molecular-therapy/abstract/S1525-0016(16)31081-4 (visited on 06/05/2026).

[18] Kalina Paunovska et al. “The Extent to Which Lipid Nanoparticles Require Apolipoprotein E and Low-Density Lipoprotein Receptor for Delivery Changes with Ionizable Lipid Structure”. eng. In: *Nano Letters* 22.24 (Dec. 2022), pp. 10025–10033. ISSN: 1530-6992. DOI: 10.1021/acs.nanolett.2c03741.

[19] *FFF Theory - Waters | Wyatt Technology*. en-US. May 2019. URL: https://www.wyatt.com/library/theory/flow-field-flow-fractionation-theory.html (visited on 05/19/2026).

[20] Katri Eskelin, Minna M. Poranen, and Hanna M. Oksanen. “Asymmetrical Flow Field-Flow Fractionation on Virus and Virus-Like Particle Applications”. en. In: *Microorganisms* 7.11 (Nov. 2019), p. 555. ISSN: 2076-2607. DOI: 10.3390/microorganisms7110555. URL: https://www.mdpi.com/2076-2607/7/11/555 (visited on 05/19/2026).

[21] Jonathan Gutow. *5.5: Stokes-Einstein-Sutherland Equation*. en. Nov. 2025. URL: https://chem.libretexts.org/Courses/University_of_Wisconsin_Oshkosh/Chem_371%3A_P-Chem_2_to_Folow_Combined_Biophysical_and_P-Chem_1_(Gutow)/05%3A_Moving_Molecules_and_Chemical_Kinetics/5.05%3A_Stokes-Einstein-Sutherland_Equation (visited on 05/19/2026).

[22] Bastian E. Rapp. *Fluids*. en-US. DOI: 10.1016/B978-1-4557-3141-1.50009-5. URL: https://www.sciencedirect.com/science/chapter/monograph/pii/B9781455731411500095 (visited on 05/19/2026).

[23] Haiyang Dou, Euo Chang Jung, and Seungho Lee. “Factors affecting measurement of channel thickness in asymmetrical flow field-flow fractionation”. In: *Journal of Chromatography A* 1393 (May 2015), pp. 115–121. ISSN: 0021-9673. DOI: 10.1016/j.chroma.2015.03.025. URL: https://www.sciencedirect.com/science/article/pii/S0021967315004082 (visited on 06/16/2026).

[24] Terry Ching et al. “Chapter 1 - Techniques and materials for the fabrication of microfluidic devices”. In: *Principles of Human Organs-on-Chips*. Ed. by Masoud Mozafari. Woodhead Publishing Series in Biomaterials. Woodhead Publishing, Jan. 2023, pp. 1–36. ISBN: 978-0-12-823536-2. DOI: 10.1016/B978-0-12-823536-2.00014-6. URL: https://www.sciencedirect.com/science/article/pii/B9780128235362000146 (visited on 06/16/2026).

[25] Bastian E. Rapp. “Chapter 11 - Conservation of Momentum: The Navier-Stokes Equation”. In: *Microfluidics: Modelling, Mechanics and Mathematics*. Micro and Nano Technologies. Oxford: Elsevier, Jan. 2017, pp. 273–289. ISBN: 978-1-4557-3141-1. DOI: 10.1016/B978-1-4557-3141-1.50011-3. URL: https://www.sciencedirect.com/science/article/pii/B9781455731411500113 (visited on 06/16/2026).

[26] Viktor P. Astakov. “High-pressure supply of metalworking fluids”. en-US. In: *Metalworking Fluids (MWFs) for Cutting and Grinding*. Woodhead Publishing, Jan. 2012, pp. 201–290. ISBN: 978-0-85709-530-5. DOI: 10.1533/9780857095305.201. URL: https://www.sciencedirect.com/science/chapter/edited-volume/pii/B9780857090614500050 (visited on 05/20/2026).

[27] Pauline M. Doran. *Fluid Flow*. en-US. DOI: 10.1016/B978-0-12-220851-5.00007-1. URL: https://www.sciencedirect.com/science/chapter/monograph/pii/B9780122208515000071 (visited on 05/20/2026).

[28] Junaid Najmi and Syed Shah. “Analysis Of Velocity Profile For Laminar Flow In A Round Pipe”. In: Nov. 2017.

[29] Brian J. Cantwell. “A universal velocity profile for smooth wall pipe flow”. en. In: *Journal of Fluid Mechanics* 878 (Nov. 2019), pp. 834–874. ISSN: 0022-1120, 1469-7645. DOI: 10.1017/jfm.2019.669. URL: https://www.cambridge.org/core/journals/journal-of-fluid-mechanics/article/universal-velocity-profile-for-smooth-wall-pipe-flow/A92AFD4518B09623A3B93E0C7E62DFE5 (visited on 05/20/2026).

[30] Herman Schlichting and Klaus Gersten. *Boundary-Layer Theory*. en. URL: https://link.springer.com/book/10.1007/978-3-662-52919-5 (visited on 05/20/2026).

[31] Jia-Lan Wang et al. “Theoretical and experimental investigation of the focusing position in asymmetrical flow field-flow fractionation (AF4)”. In: *Journal of Chromatography A* 1561 (Aug. 2018), pp. 67–75. ISSN: 0021-9673. DOI: 10.1016/j.chroma.2018.04.056. URL: https://www.sciencedirect.com/science/article/pii/S002196731830517X (visited on 05/20/2026).

[32] Anne Litzén and Karl-Gustav Wahlund. *Zone broadening and dilution in rectangular and trapezoidal asymmetrical flow field-flow fractionation channels*. en. May 1991. URL: https://pubs.acs.org/doi/abs/10.1021/ac00010a013 (visited on 05/19/2026).

[33] Jeffrey D. Clogston and Yingwen Hu. “Asymmetric-Flow Field-Flow Fractionation”. en. In: *National Cancer Institute’s Nanotechnology Characterization Laboratory Assay Cascade Protocols [Internet]*. National Cancer Institute (US), May 2020. DOI: 10.17917/8S1D-BN17. URL: https://www.ncbi.nlm.nih.gov/books/NBK604931/ (visited on 05/18/2026).

[34] Catalina Fuentes et al. “Comparison between conventional and frit-inlet channels in separation of biopolymers by asymmetric flow field-flow fractionation”. en. In: *Analyst* 144.15 (July 2019), pp. 4559–4568. ISSN: 1364-5528. DOI: 10.1039/C9AN00466A. URL: https://pubs.rsc.org/en/content/articlelanding/2019/an/c9an00466a (visited on 06/01/2026).

[35] Juan Bian et al. “The Power of Field-Flow Fractionation in Characterization of Nanoparticles in Drug Delivery”. In: *Molecules* 28.10 (May 2023), p. 4169. ISSN: 1420-3049. DOI: 10.3390/molecules28104169. URL: https://pmc.ncbi.nlm.nih.gov/articles/PMC10224342/ (visited on 06/01/2026).

[36] Maria Marioli and Wim Th. Kok. “Recovery, overloading, and protein interactions in asymmetrical flow field-flow fractionation”. In: *Analytical and Bioanalytical Chemistry* 411.11 (2019), pp. 2327–2338. ISSN: 1618-2642. DOI: 10.1007/s00216-019-01673-w. URL: https://pmc.ncbi.nlm.nih.gov/articles/PMC6459789/ (visited on 05/22/2026).

[37] *Eclipse NEON - Waters | Wyatt Technology*. en-US. Aug. 2020. URL: https://www.wyatt.com/products/instruments/eclipse-field-flow-fractionation-system.html (visited on 05/22/2026).

[38] *MALS Theory - Waters | Wyatt Technology*. en-US. May 2019. URL: https://www.wyatt.com/library/theory/multi-angle-light-scattering-theory.html (visited on 05/22/2026).

[39] Ephraim Shahmoon and Gershon Kurizki. “Nonlinear theory of laser-induced dipolar interactions in arbitrary geometry”. In: *Physical Review A* 89.4 (Apr. 2014). arXiv:1311.0568 [quant-ph], p. 043419. ISSN: 1050-2947, 1094-1622. DOI: 10.1103/PhysRevA.89.043419. URL: http://arxiv.org/abs/1311.0568 (visited on 05/22/2026).

[40] *How It Works: UV Detection for HPLC | LCGC International*. en. May 2026. URL: https://www.chromatographyonline.com/view/how-it-works-uv-detection-hplc?utm_source=chatgpt.com (visited on 05/23/2026).

[41] Samuel Montero. *Molar absorption coefficient – openfnirs*. en-US. Jan. 2024. URL: https://openfnirs.org/2024/01/01/molar-absorption-coefficient/ (visited on 05/23/2026).

[42] Hitachi High-Tech. *8. Principle and Feature of Various Detection Methods (2)*. en. URL: https://www.hitachi-hightech.com/global/en/knowledge/analytical-systems/hplc/hplc-basics/course8.html (visited on 06/02/2026).

[43] *How HPLC Detectors Work - SE*. en. URL: https://www.thermofisher.com/uk/en/home/industrial/chromatography/chromatography-learning-center/liquid-chromatography-information/hplc-system-components/how-hplc-detectors-work.html (visited on 06/02/2026).

[44] R.P.W. Scott. “Chapter 2 The Refractive Index Detector”. en-US. In: *Journal of Chromatography Library*. Vol. 11. Elsevier, Jan. 1977, pp. 59–67. DOI: 10.1016/S0301-4770(08)61012-X. URL: https://www.sciencedirect.com/science/chapter/bookseries/pii/S030147700861012X (visited on 06/02/2026).

[45] *What is Mass Spectrometry?* en. Sept. 2010. URL: https://www.broadinstitute.org/technology-areas/what-mass-spectrometry (visited on 05/23/2026).

[46] Susan R Mikkelsen and Eduardo Corton. *Bioanalytical Chemistry*. (Visited on 05/23/2026).

[47] *6.6: Centripetal Force*. en. Oct. 2016. URL: https://phys.libretexts.org/Bookshelves/University_Physics/University_Physics_(OpenStax)/Book%3A_University_Physics_I_-_Mechanics_Sound_Oscillations_and_Waves_(OpenStax)/06%3A_Applications_of_Newton's_Laws/6.06%3A_Centripetal_Force (visited on 05/25/2026).

[48] *Magnetic Force Between Two Parallel Current Carrying Wires*. en-GB. URL: https://utk.instructuremedia.com/embed/c4ab12fa-ab8e-44d8-b992-4cbfe5c11c87 (visited on 05/25/2026).

[49] W. M. A. Niessen. "MS-MS and MSn". In: *Encyclopedia of Spectroscopy and Spectrometry*. Ed. by John C. Lindon. Oxford: Elsevier, Jan. 1999, pp. 1404–1410. ISBN: 978-0-12-226680-5. DOI: 10.1006/rwsp.2000.0186. URL: https://www.sciencedirect.com/science/article/pii/B0122266803001861 (visited on 06/07/2026).

[50] Krzysztof Selinger, Eliza N. Fung, and Peter Bryan. "Chapter 16 - Bioanalytical method validation and bioanalysis in regulated settings". In: *Specification of Drug Substances and Products*. Ed. by Christopher M. Riley, Thomas W. Rosanske, and Shelley R. Rabel Riley. Oxford: Elsevier, Jan. 2014, pp. 325–363. ISBN: 978-0-08-098350-9. DOI: 10.1016/B978-0-08-098350-9.00016-3. URL: https://www.sciencedirect.com/science/article/pii/B9780080983509000163 (visited on 06/07/2026).

[51] Ting Huang et al. "Protein inference: a review". In: *Briefings in Bioinformatics* 13.5 (Sept. 2012), pp. 586–614. ISSN: 1467-5463. DOI: 10.1093/bib/bbs004. URL: https://doi.org/10.1093/bib/bbs004 (visited on 06/08/2026).

[52] Manfred Claassen. "Inference and Validation of Protein Identifications". In: *Molecular & Cellular Proteomics : MCP* 11.11 (Nov. 2012), pp. 1097–1104. ISSN: 1535-9476. DOI: 10.1074/mcp.R111.014795. URL: https://pmc.ncbi.nlm.nih.gov/articles/PMC3494198/ (visited on 06/08/2026).

[53] Nijin Wu et al. "Albumin, an interesting and functionally diverse protein, varies from 'native' to 'effective' (Review)". In: *Molecular Medicine Reports* 29.2 (Dec. 2023), p. 24. ISSN: 1791-2997. DOI: 10.3892/mmr.2023.13147. URL: https://pmc.ncbi.nlm.nih.gov/articles/PMC10784728/ (visited on 06/08/2026).

[54] Rajiv Rose and Harold G Klemcke. "Relationship between Plasma Albumin Concentration and Plasma Volume in 5 Inbred Rat Strains". In: *Journal of the American Association for Laboratory Animal Science : JAALAS* 54.5 (Sept. 2015), pp. 459–464. ISSN: 1559-6109. URL: https://pmc.ncbi.nlm.nih.gov/articles/PMC4587612/ (visited on 06/08/2026).

[55] Hyeran Noh and Erwin A. Vogler. "Volumetric interpretation of protein adsorption: Competition from mixtures and the Vroman effect". In: *Biomaterials* 28.3 (Jan. 2007), pp. 405–422. ISSN: 0142-9612. DOI: 10.1016/j.biomaterials.2006.09.006. URL: https://www.sciencedirect.com/science/article/pii/S0142961206007964 (visited on 06/21/2026).

[56] Lisa M. Kobos et al. "An Integrative Proteomic/Lipidomic Analysis of the Gold Nanoparticle Biocorona in Healthy and Obese Conditions". In: *Applied in Vitro Toxicology* 5.3 (Sept. 2019), pp. 150–166. ISSN: 2332-1512. DOI: 10.1089/aivt.2019.0005. URL: https://pmc.ncbi.nlm.nih.gov/articles/PMC6768227/ (visited on 07/06/2026).

10 Appendix

10.1 Figures

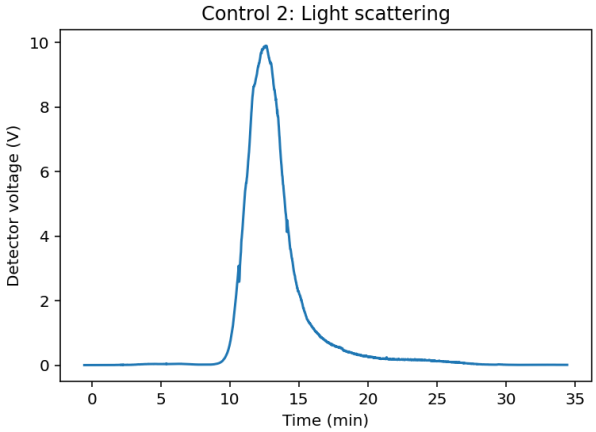

Figure 10.1: Light scattering at a 90^o angle from the incident beam for Control 2 throughout the separation process.

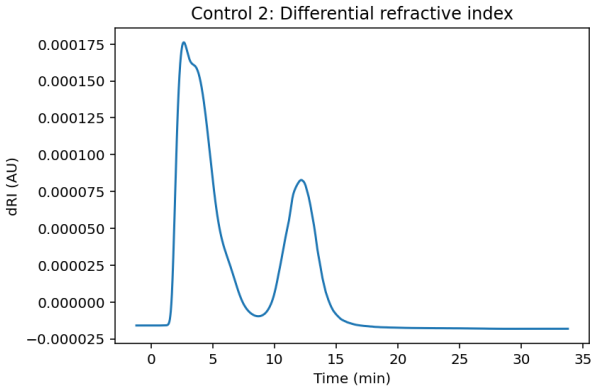

Figure 10.2: Differential refractive index for Control 2 throughout the separation process.

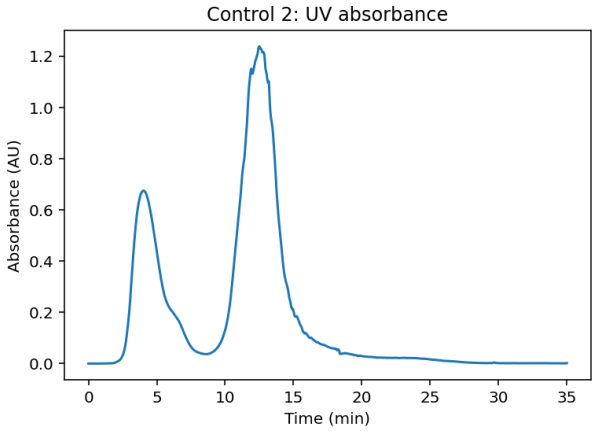

Figure 10.3: UV absorption for Control 2 throughout the separation process.

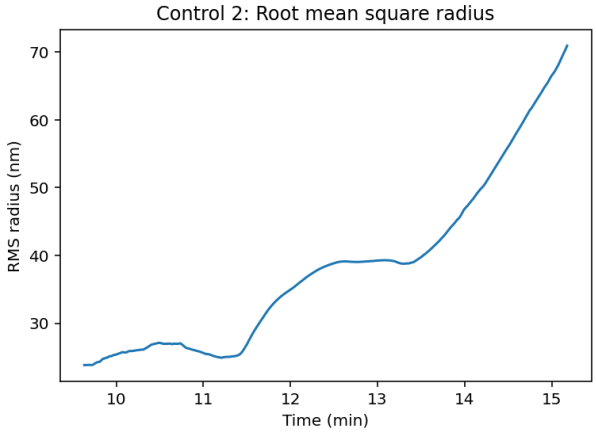

Figure 10.4: Root mean square radius for Control 2 over the time of the protein peak. The exact length in the x-direction for each injection depends only on the manually placed peak intervals in Astra.

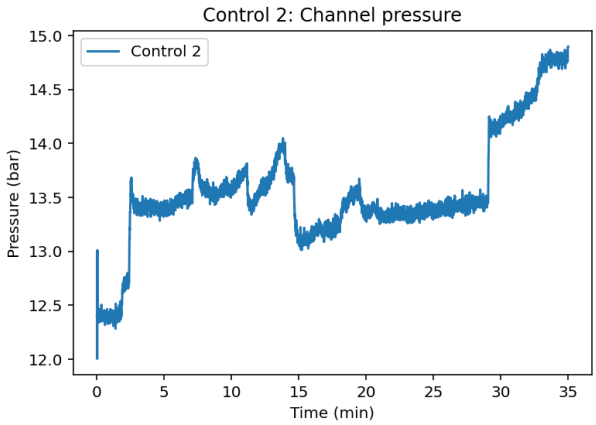

Figure 10.5: Channel pressure for Control 2 throughout the separation process.

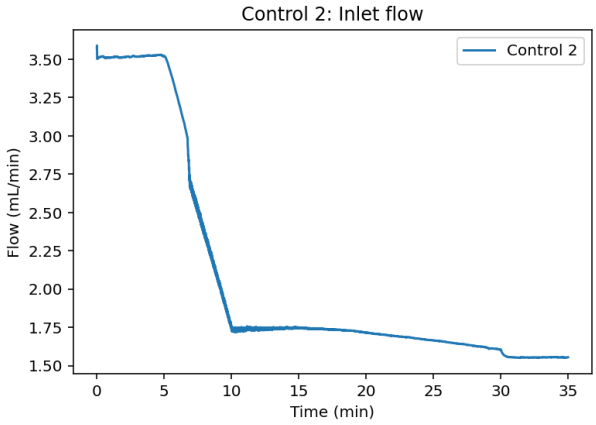

Figure 10.6: Inlet flow for Control 2 throughout the separation process.

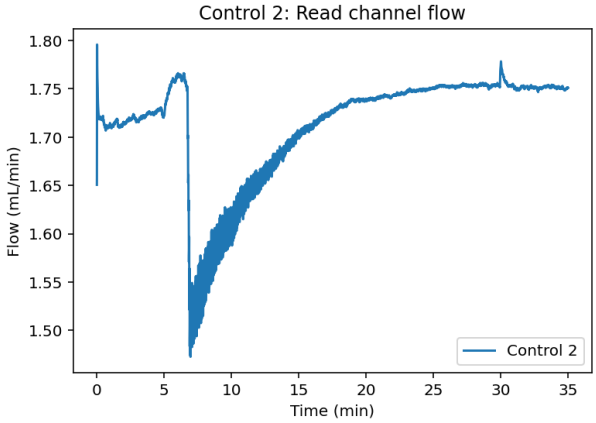

Figure 10.7: Read channel flow for Control 2 throughout the separation process.

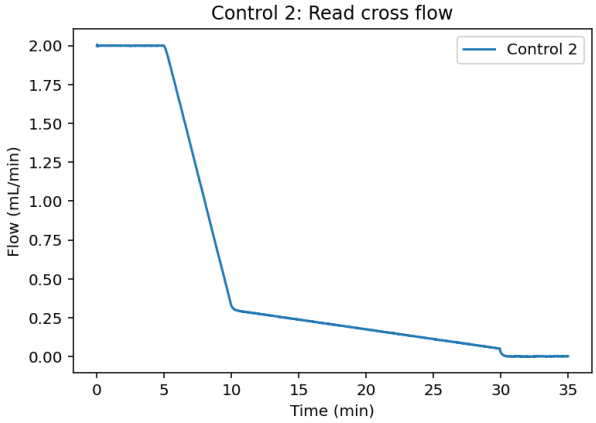

Figure 10.8: Read cross flow for Control 2 throughout the separation process.

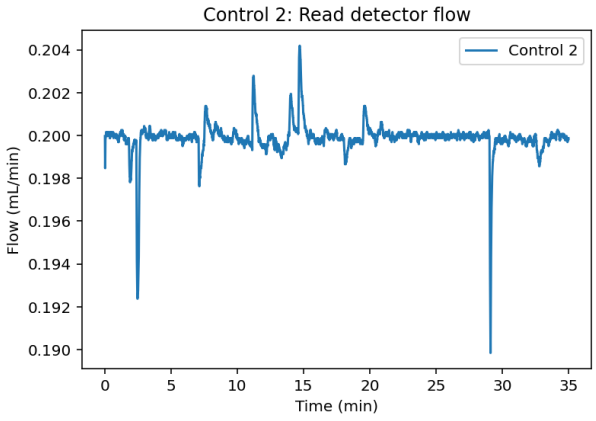

Figure 10.9: Read detector flow for Control 2 throughout the separation process.

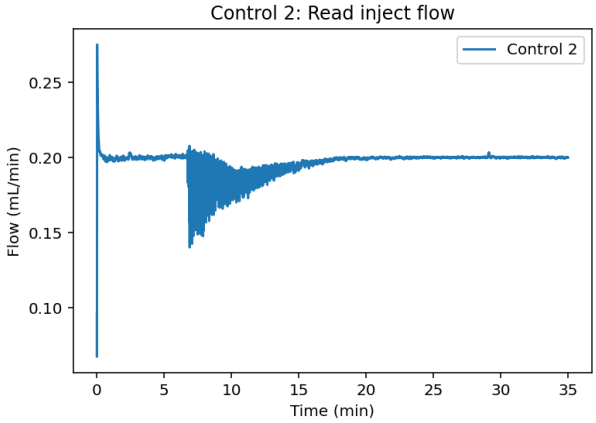

Figure 10.10: Read inject flow for Control 2 throughout the separation process.

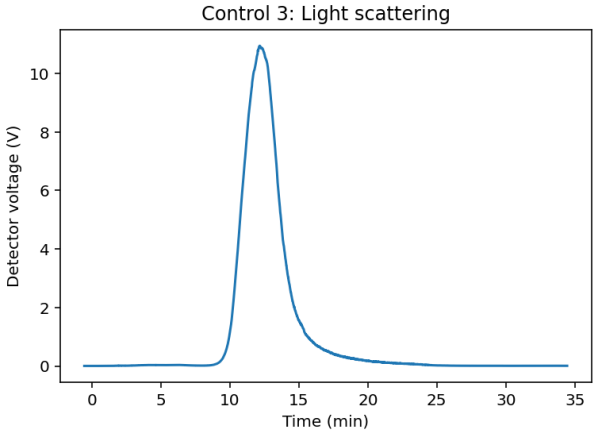

Figure 10.11: Light scattering at a 90^o angle from the incident beam for Control 3 throughout the separation process.

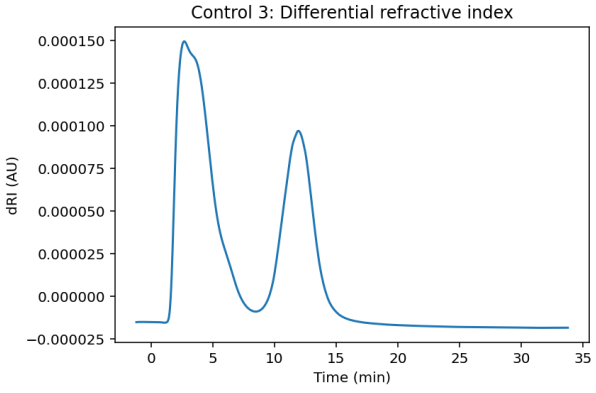

Figure 10.12: Differential refractive index for Control 3 throughout the separation process.

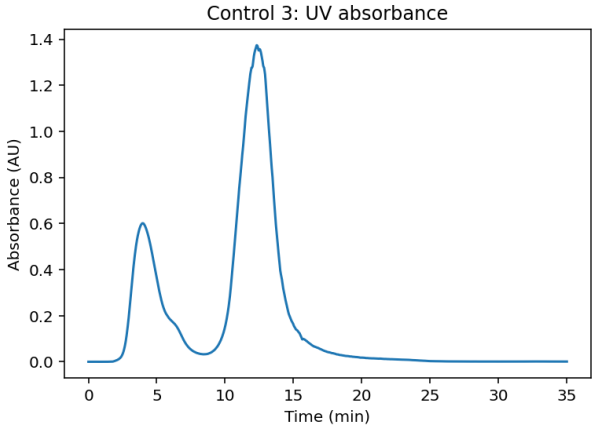

Figure 10.13: UV absorption for Control 3 throughout the separation process.

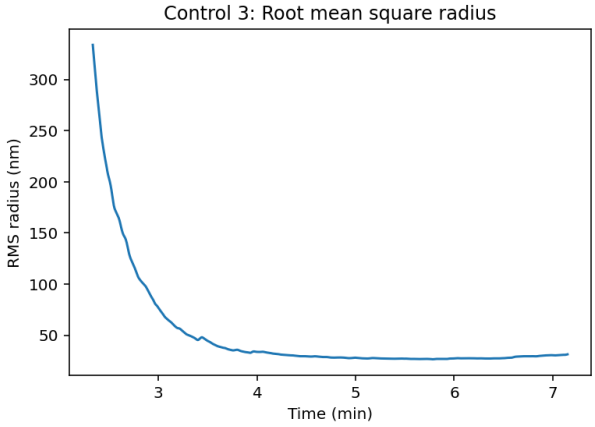

Figure 10.14: Root mean square radius for Control 3 over the time of the protein peak. The exact length in the x-direction for each injection depends only on the manually placed peak intervals in Astra.

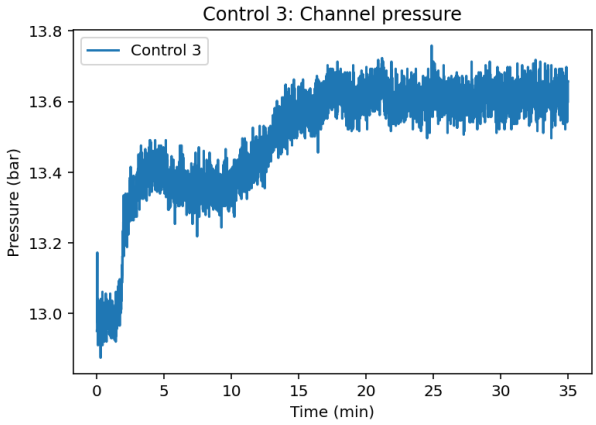

Figure 10.15: Channel pressure for Control 3 throughout the separation process.

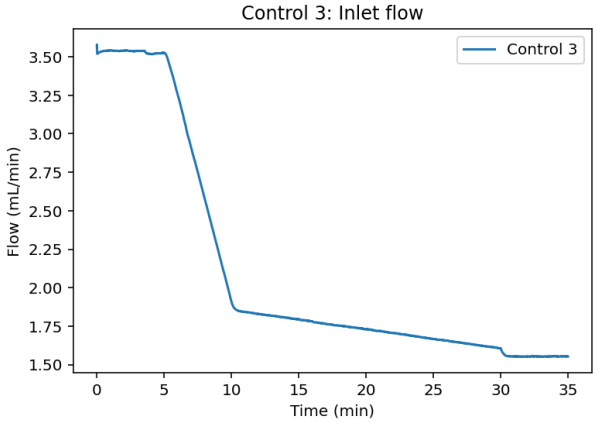

Figure 10.16: Inlet flow for Control 3 throughout the separation process.

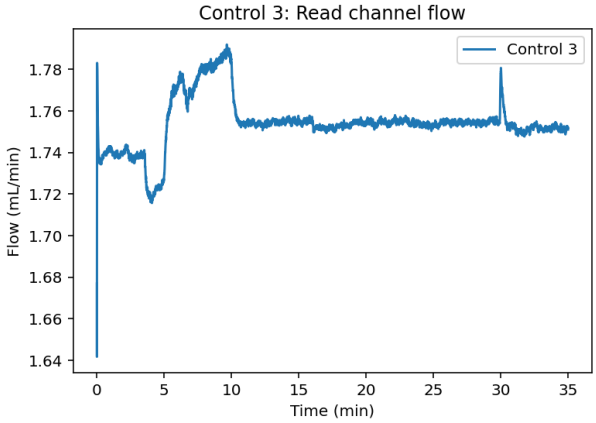

Figure 10.17: Read channel flow for Control 3 throughout the separation process.

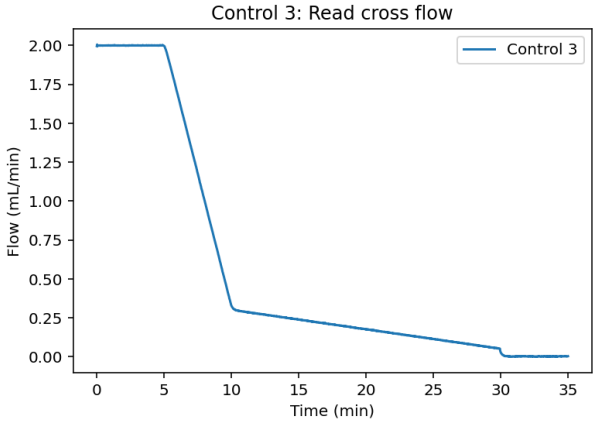

Figure 10.18: Read cross flow for Control 3 throughout the separation process.

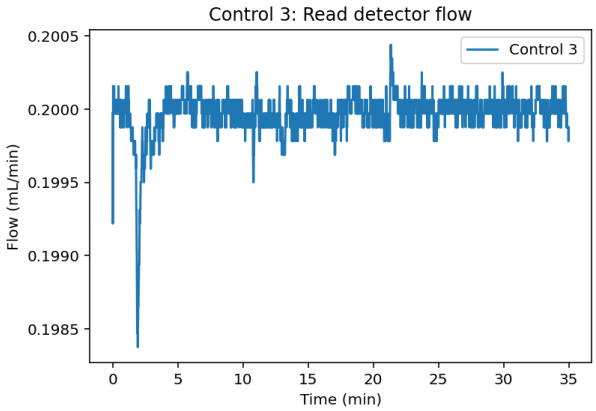

Figure 10.19: Read detector flow for Control 3 throughout the separation process.

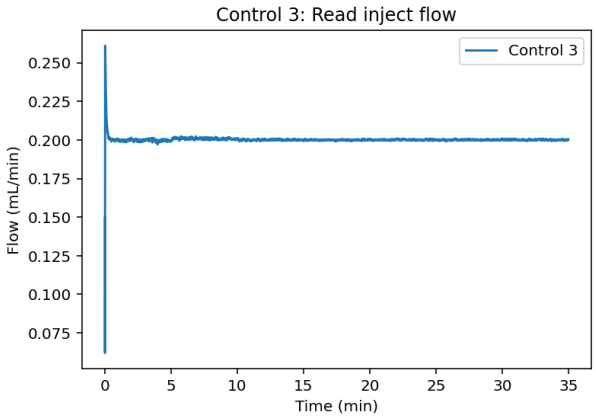

Figure 10.20: Read inject flow for Control 3 throughout the separation process.

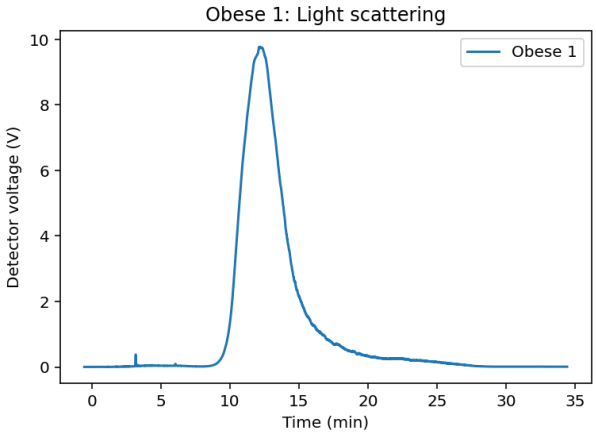

Figure 10.21: Light scattering at a 90^{o} angle from the incident beam for Obese 1 throughout the separation process.

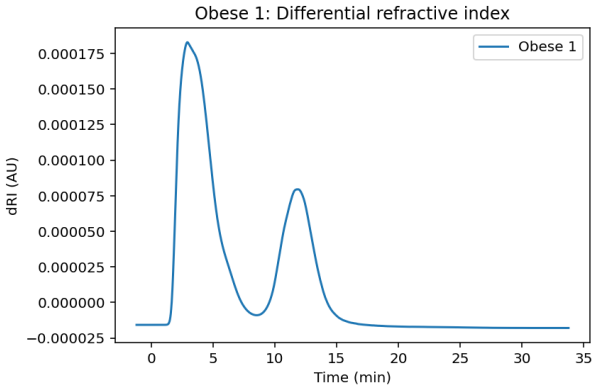

Figure 10.22: Differential refractive index for Obese 1 throughout the separation process.

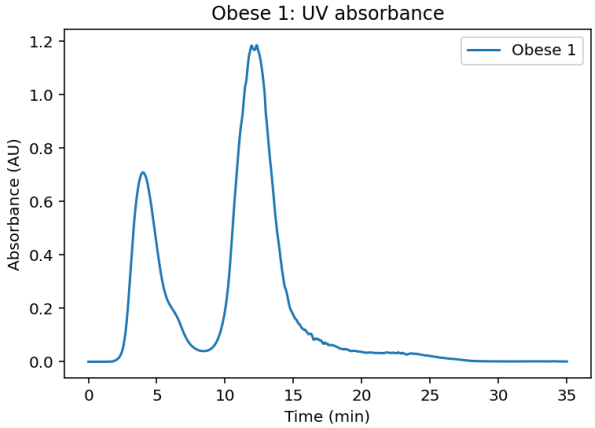

Figure 10.23: UV absorption for Obese 1 throughout the separation process.

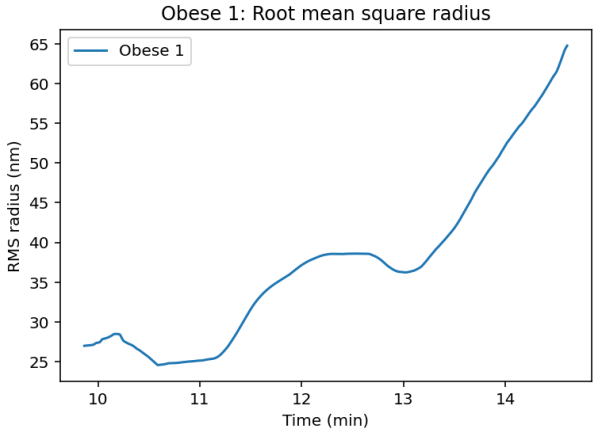

Figure 10.24: Root mean square radius for Obese 1 over the time of the protein peak. The exact length in the x-direction for each injection depends only on the manually placed peak intervals in Astra.

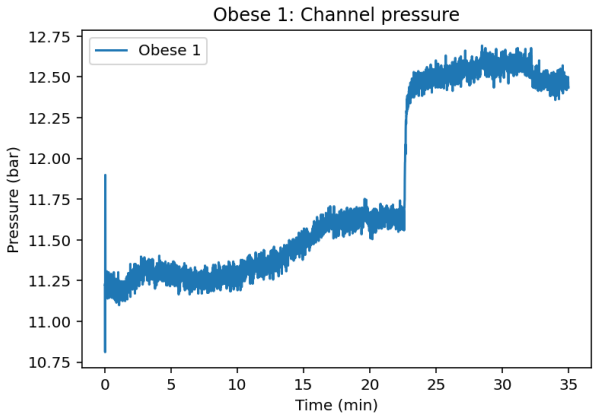

Figure 10.25: Channel pressure for Obese 1 throughout the separation process.

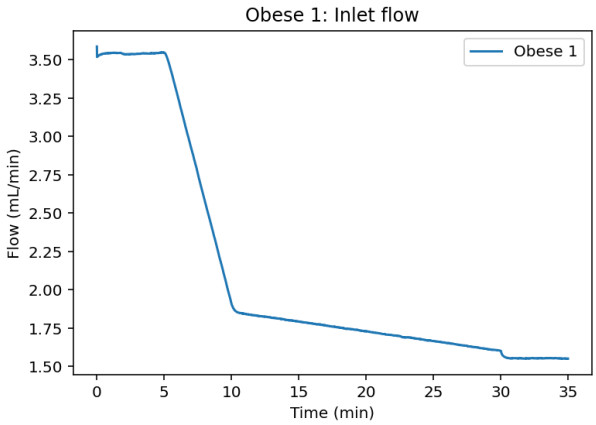

Figure 10.26: Inlet flow for Obese 1 throughout the separation process.

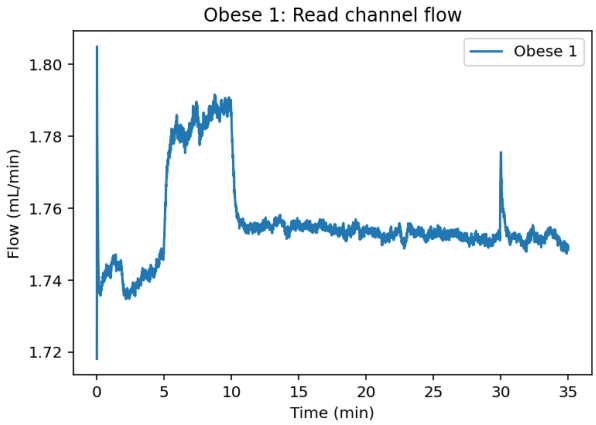

Figure 10.27: Read channel flow for Obese 1 throughout the separation process.

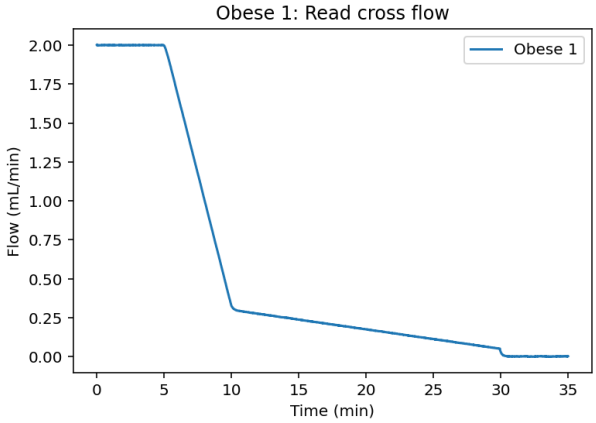

Figure 10.28: Read cross flow for Obese 1 throughout the separation process.

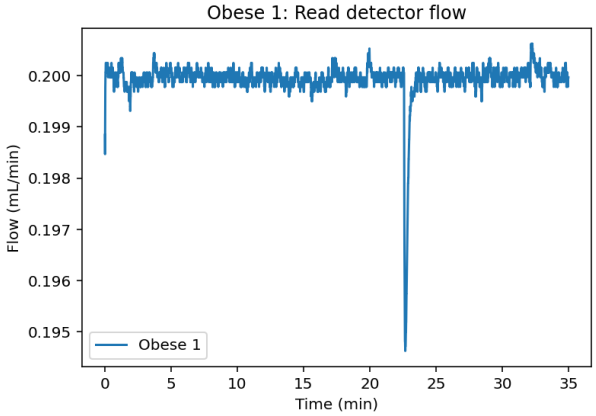

Figure 10.29: Read detector flow for Obese 1 throughout the separation process.

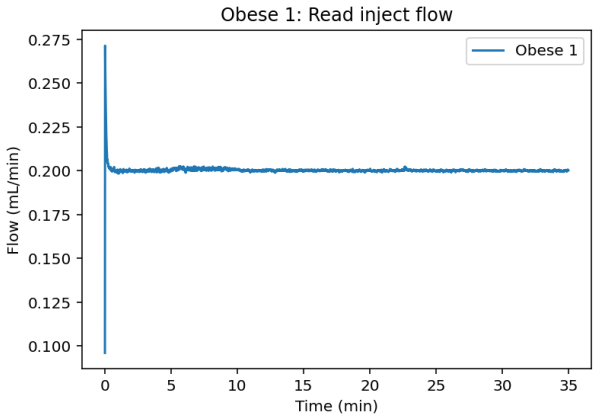

Figure 10.30: Read inject flow for Obese 1 throughout the separation process.

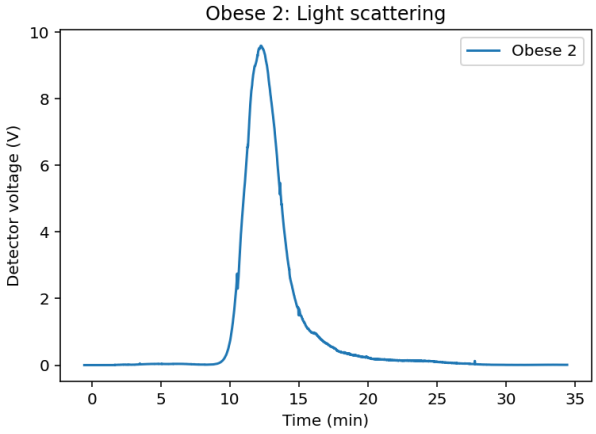

Figure 10.31: Light scattering at a 90^o angle from the incident beam for Obese 2 throughout the separation process.

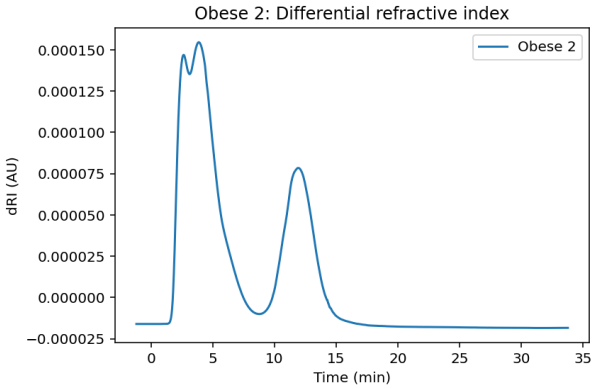

Figure 10.32: Differential refractive index for Obese 2 throughout the separation process.

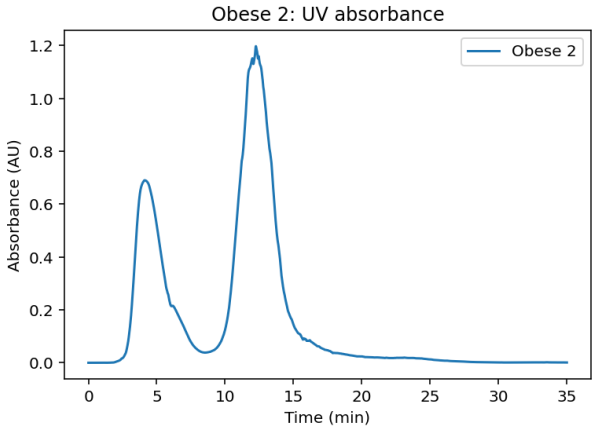

Figure 10.33: UV absorption for Obese 2 throughout the separation process.

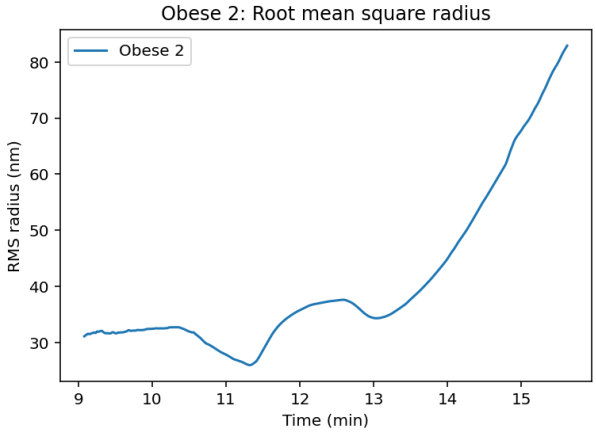

Figure 10.34: Root mean square radius for Obese 2 over the time of the protein peak. The exact length in the x-direction for each injection depends only on the manually placed peak intervals in Astra.

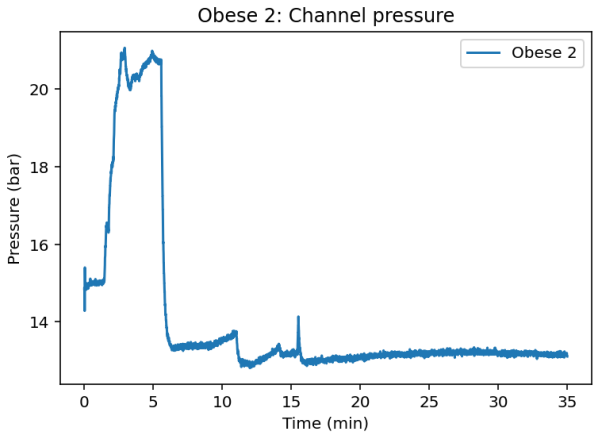

Figure 10.35: Channel pressure for Obese 2 throughout the separation process.

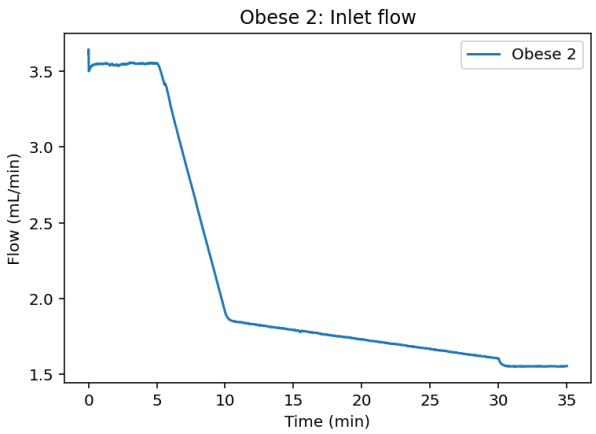

Figure 10.36: Inlet flow for Obese 2 throughout the separation process.

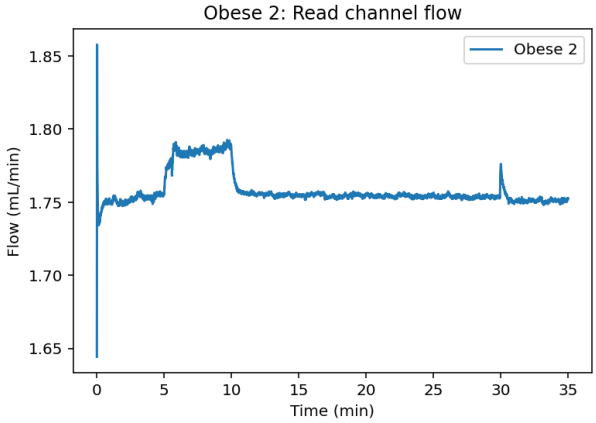

Figure 10.37: Read channel flow for Obese 2 throughout the separation process.

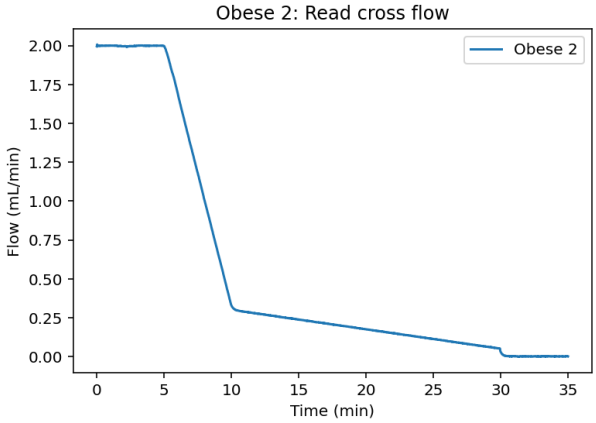

Figure 10.38: Read cross flow for Obese 2 throughout the separation process.

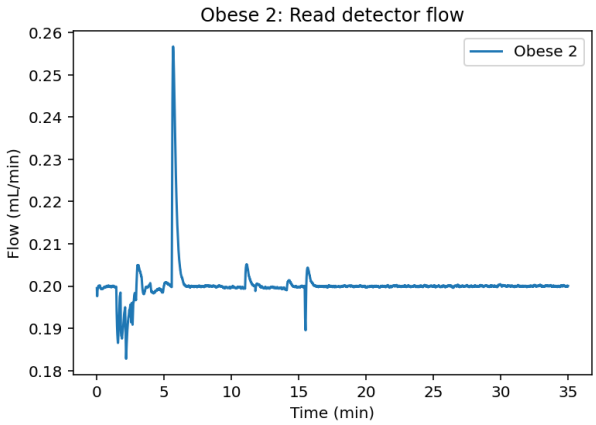

Figure 10.39: Read detector flow for Obese 2 throughout the separation process.

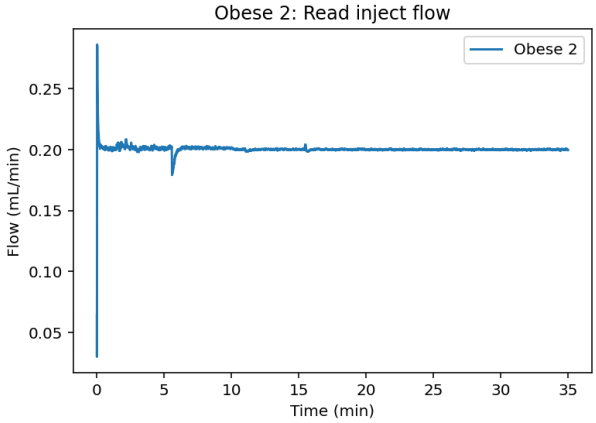

Figure 10.40: Read inject flow for Obese 2 throughout the separation process.